High-Throughput Pressure Dependent DFT Investigation of Herringbone Polycyclic Aromatic Hydrocarbons (HB-PAHs): Part 2. Pressure Dependent Electronic Properties

Mahmoud Hammouri^a, Taylor Garcia^b, Cameron Cook^a, Stephen Monaco^b, Sebastian Jezowski^c Noa Marom^d, and Bohdan Schatschneider^{a,b*}

Abstract: Understanding the effect intermolecular interactions have on the electronic properties of highly conjugated/aromatic organic networks is important for optimizing these materials for optoelectronic device applications. Here, we use dispersion inclusive density functional theory (DFT+vdW) to study the effect of pressure up to 20 GPa on the intermolecular interactions of 42 herringbone (HB) polycyclic aromatic hydrocarbons (PAHs). In the first part of this two-part study, we reported the pressure induced structural changes. Here, we elucidate the relation between these structural changes and the electronic properties. Increased pressure leads to variations in the intermolecular interactions and molecular conformations, resulting in alterations of the band dispersion, band gap (magnitude as well as direct/indirect), and semiconductor polarity (*n*-type vs. *p*-type). Specifically, increased pressure increases the C-H··· π and π ··· π interactions, typically leading to increased intermolecular orbital overlap of the frontier molecular orbitals, resulting in increased intermolecular coupling and band dispersion. In general, the increased intermolecular coupling and band dispersion yield decreased band gaps and increased crystalline polarizabilities, although some variation in these trends occur. The majority of structures follow similar trends. However, some exhibit anomalous pressure responses, including switching between n-type and p-type polarity, transitions between direct/indirect gaps, and discontinuities in the pressure dependent band gap curves.

^a California State Polytechnic University at Pomona, 3801 W Temple Ave, Pomona, CA 91768 United States

^b The Pennsylvania State University, Fayette-The Eberly Campus, 2201 University Drive, Lemont Furnace, Pennsylvania 15456, United States

^c Department of Chemistry, Murry State University, 102 Curris Center, Murry, KY 42071

^dDepartment of Materials Science and Engineering, Department of Physics, and Department of Chemistry, Carnegie Mellon University, 5000 Forbes Avenue, Pittsburgh, PA 15213-3890

1. Introduction: The ever-expanding push to utilize mixed and single component organic molecular networks in optoelectronic applications has created a significant demand for organic materials with extraordinary properties. It is postulated that the synthesis of useful organic-electronic materials would be a significant "green" advance for electronic devices owing to lower material costs and increased ease of production. Crystalline organic semiconductors have shown promise in a wide range of device applications, ²⁻¹³ but further refinement of the electronic properties through molecular- and/or crystal-engineering is needed to enhance long term applicability and optimize device performance. One promising class of organic semiconductors is polycyclic aromatic hydrocarbons (PAHs). PAHs are a group of non-polar organic compounds comprised primarily of carbon and hydrogen, arranged in aromatic rings. PAHs have potential for use in electronic devices due to their high stabilities, electron transport capabilities, and potential superconductivity. PAHs may contain heteroatoms which can significantly perturb the electronic properties of the material. Owing to the large properties variability in heterocyclic structures, we have chosen to focus on PAHs containing only C and H for ease of comparison.

Semiconducting PAHs have been used in a wide range of applications including transistors, diodes, and solar cells. $^{7-12}$ In organic light emitting diodes (OLEDs), recombination of electrons and holes across the band gap (E_g) leads to photoemission. 13,14 Conversely, in organic photovoltaics (OPV) the absorption of photons leads to electron excitations across E_g , resulting in charge carrier and electrical current generation. In both cases, the magnitude and direct/indirect nature of E_g has significant importance. In OPV, a small E_g is preferred as lower excitation energies can provide for energy absorption across a broader spectrum. In OLEDs, E_g can be tuned in order to alter the color of the emitted light. A direct E_g is preferred in both devices because excitation/relaxation across an indirect gap requires coupling to phonons in order to account for the change in momentum, resulting in energy loss. Tuning of E_g , and switching between direct/indirect gaps, is currently a coveted target in molecular- and crystal-engineering as it has the potential to result in more efficient devices with tailored properties.

External pressure has been shown both theoretically and experimentally to alter E_g in crystalline PAHs, such as poly(para-phenylenes), ¹⁵ picene, ¹⁶ oligoacenes, ^{17,18} triphenylene, ¹⁹ and rubrene²⁰ by modifying the intermolecular interactions and molecular conformations. In PAHs, pressure is known to induce polymorphic phase transitions and can change other properties (e.g., aromatic character) of the molecular components that are ultimately linked to the electronic properties of the crystals. Such changes have been shown to increase the internal energy and enthalpy of the system, reducing the aromaticity and changing the band gap.²¹ Moreover, increased charge carrier mobilities in organic semiconductor devices have been achieved experimentally by applying hydrostatic pressure. 19,22-26 For example, in crystalline benz[a]anthracene photocurrent has been shown to increase with increased pressure, along with a reversible color change.²⁷ A recent first-principle study of the phenacene family revealed a linear increase in the hole and electron mobilities with increasing pressure, as well as switching between *n*- and *p*-type semiconductor behavior.²⁶ The hole mobility of all three systems was found to surpass that of amorphous Si around 9.3 GPa, 6 GPa, and 2 GPa for phenanthrene, chrysene, and picene, respectively. Additionally, chrysene was found to convert from n-type polarity, to ambipolar, to p-type via band structure analysis over the 0 to 3 GPa range. The ability to control E_g as well as other electronic properties in solid PAHs via engineering of the intermolecular interactions could result in significant advancement of their applications in organic electronic devices.

PAHs exhibit five typical crystalline packing motifs: 1) herringbone (HB) 2) sandwich herringbone (SHB) 3) beta herringbone (β-HB) 4) beta (β) and 5) Gamma (γ). Each motif is characterized *via* the percent C···C intermolecular interactions present on the Hirshfeld surface and the interplanar angle between neighboring molecules. Among the five arrangements, the herringbone (HB) motif is the most common and is described as having primarily edge-to-face (C···H) and edge-to-edge (H···H) interactions with a very small amount of cofacial (π ··· π /C···C) contacts. The relatively weak van der Waals (vdW) forces binding HB-PAHs allow for easy perturbation of the crystalline structure with low-to-moderate pressures, and in some cases enables the evolution of new polymorphs and physical properties. He present a comprehensive study of the behavior of 42 HB-PAHs under the influence of isotropic pressure up to 20 GPa, using dispersion inclusive density functional theory (DFT+vdW). Pressure dependent structural trends were reported in the first part of this study. This paper explores the corresponding pressure induced changes in the electronic properties of HB-PAHs.

2. Computational Methods

DFT calculations were conducted using the Perdew-Burke-Ernzerhof (PBE) generalized gradient approximation³⁷ with the pairwise dispersion scheme of Tkatchenko–Scheffler (TS).³⁸ The reliability of PBE+vdW for modeling the structure and electronic properties of PAHs has been established in our previous work.³⁹ Therein, it was shown that the variation between the calculated mass densities, unit cell parameters, and Hirshfeld intermolecular close contact fractions were within +5%, $\pm2\%$, and $\pm1\%$ of experiment, respectively. Our previous high pressure work on oligoacenes,¹⁷ rubrene,²⁰ indole,³² and TCNE⁴⁰ shows that PBE+vdW can accurately model the pressure dependent structural response of molecular crystals that exhibit a variety of intermolecular forces.²⁴ Therefore, we are reasonably confident that the predicted high pressure structures presented here offer realistic insight into the pressure response of the HB-PAH group.

Band gaps were calculated using PBE and the PBE-based hybrid functional (PBE0)⁴¹. The hybrid functional PBE0 was used in some instances to mitigate the underestimation of the band gap by PBE. We have shown in a previous ambient pressure investigation on PAHs that addition of a 1.05 eV constant to the PBE+vdW E_g values (E_g^{PBE}) results in excellent agreement with experimentally determined optical gaps (E_g^{opt}).³⁹ We have further demonstrated that PBE+vdW can reliably model the pressure dependent E_g trends of HB-PAHs.^{17,20} Comparison of experimental high pressure data¹⁶ for E_g^{opt} and E_g^{PBE} of picene (ZZZOYC01) provided in **SI Fig S1** shows clearly that excellent agreement at high pressure is achievable by adding the 1.05 eV constant. Based on the performance of PBE+vdW for describing the ambient and high pressure electronic-structure trends of PAHs in the aforementioned studies, and the correlation of our calculated structures with new pressure dependent experimental data, we are confident that the pressure dependent physicochemical trends reported here are reliable, and that values for the optical gaps of these systems can be estimated *via* addition of a 1.05 eV constant.

From the standpoint of a high-throughput investigation, in which ~1700 calculations were performed on fairly large periodic systems, a balance between chemical accuracy, reproducibility, comparability, and speed needed to be met. This can be ensured by selecting a standard set of input parameters for all calculations, which has provided reliable results in previous investigations. The Cambridge Serial Total Energy Package (CASTEP) electronic structure code was used, where all of the electronic wave functions are expanded in a planewave basis set with periodic boundary conditions. The plane-wave cutoff energy was set to 750

eV. Other convergence criteria were set as follows: total energy, max force, max stress, max displacement, and SCF iterations are 5 x 10^{-6} eV/atom, 0.01 eV/Å, 0.02 GPa, 5×10^{-4} Å⁻¹ and 5×10^{-7} eV/atom, respectively. For the *k*-point sampling, we chose the Monkhorst-Pack⁴³ scheme, such that the *k*-point separation is about 0.07 Å⁻¹ for the geometry optimizations.

For the band structure calculations, a tighter k-point spacing of $\sim 0.015~\text{Å}^{-1}$ was selected. CASTEP optimizes the k-point mesh according to the system symmetry to create the smallest even number of k-points that satisfies the target spacing. Additionally, CASTEP has a flag called NEXTRA_BANDS that controls the number of bands calculated above the Fermi level (E_F). This feature was used to enhance the speed of the calculations by limiting the number of bands above E_F to 12. The energies of the bands calculated using the NEXTRA_BAND option are the same as when calculated without that option specified as shown in **SI-Figure S11**. Norm-conserving pseudopotentials from the Open-source Pseudopotential Interface and Unification Module (OPIUM), in which the RRKJ optimized method⁴⁴ is implemented, were employed for C and H atoms.

The geometry (lattice parameters and atomic coordinates) of the PAH crystal structures were optimized at pressures up to 20 GPa in 0.5 GPa increments with the Broyden–Fletcher–Goldfarb–Shanno (BFGS) minimizer, which uses a starting Hessian that is recursively updated during optimization.⁴⁵ The starting structures were obtained from the data sets available in the Cambridge Structural Database (CSD). All structures are referred to using their 6 to 8 letter CSD reference codes (*e.g.*, benzene = BENZEN or naphthalene = NAPANT04). A table of all structures and names is provided in the SI. All geometry optimized structures and properties have been uploaded to the Organic Crystal Structure and Electronic Properties Database (OCSEPD) at organic crystal bandgaps.org.

Hirshfeld surfaces and the corresponding fingerprint plots were generated using Crystal Explorer 3.0.⁴⁶ For the intermolecular interactions within the crystal structures, we constructed fingerprint plots *via* Hirshfeld surface deconvolution.^{47,48,49} Hirshfeld surface analysis has been used previously as a powerful tool for determining intermolecular interactions within molecular crystals^{17,28,32}

3.1 Pressure dependent Band Gap Analysis

3.1.1 General Band Gap Pressure Dependence of HB-PAHs.

High pressure can increase charge carrier mobilities and reduce the band gap (E_g) of molecular crystals via two mechanisms. The first is increasing the band dispersion by enhancing molecular orbital (MO) overlap and the second is deformation of the molecular conformation, leading to changes in the single molecule MO energies, hereafter referred to as the band origin energies. Because the spacing between molecules in the solid is reduced at elevated pressures, there is typically an increase in intermolecular electronic coupling. As a result, at elevated pressures it is generally found that the eigenstates contributing to the band structure are more dispersed along certain paths in k-space. This typically leads to a direct pressure dependence of the bandwidth. As a result of the increased bandwidth, the lowest energy eigenstate of the conduction band (associated with the LUMO) will have a lower energy minimum, and the highest energy eigenstate of the valence band (associated with the HOMO) will have a higher energy maximum, creating a reduction in E_g (exceptions to this trend are discussed in detail below). Similar effects are observable as a function of temperature: As the temperature is decreased and the density of the material increases, the MO overlap increases and the band dispersion becomes larger. As

Conversely, pressure induced intermolecular interactions in organic molecular crystals have been shown to perturb the molecular geometry of the individual components. Pressure induced changes of intramolecular bonds or intramolecular bond angles can alter bond stabilization energies within the molecule. This may lead to changes in the band origin energies with respect to low pressure, resulting in E_g expansion or contraction. These pressure induced structural changes, and the ensuing changes in the electronic structures, could help produce new polymorphs with enhanced electronic and optical properties for device applications.

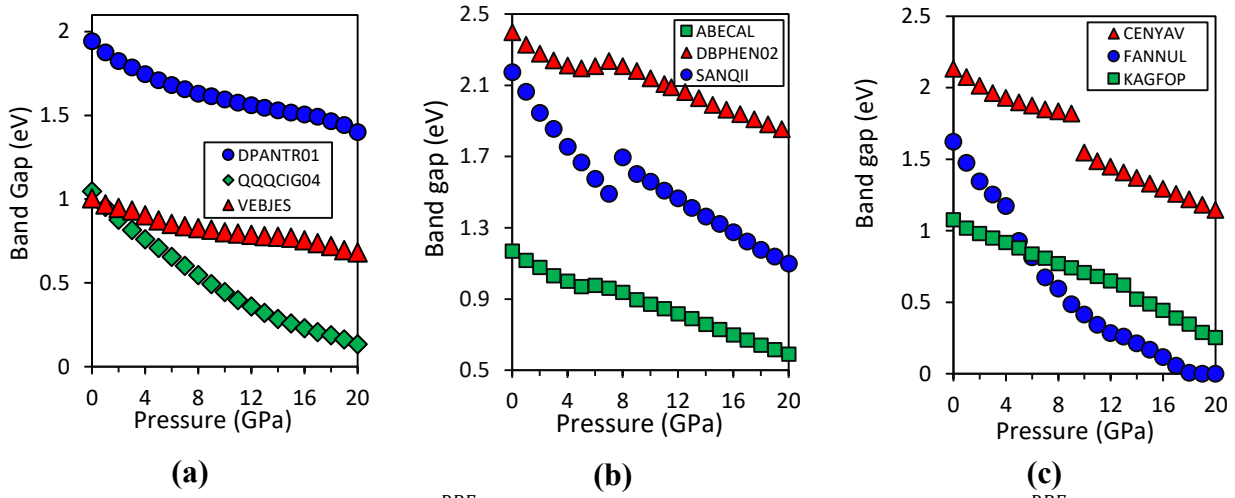


Figure 1. Pressure dependence of E_g^{PBE} for several HB-PAHs. a) Continuous decrease in E_g^{PBE} as a function of pressure for aryl oligoacenes derivatives (cruciforms). b) Discontinuous increases in E_g^{PBE} as a function of pressure. c) Discontinuous decreases in E_g^{PBE} as a function of pressure. Crystals are denoted by their CSD reference codes.

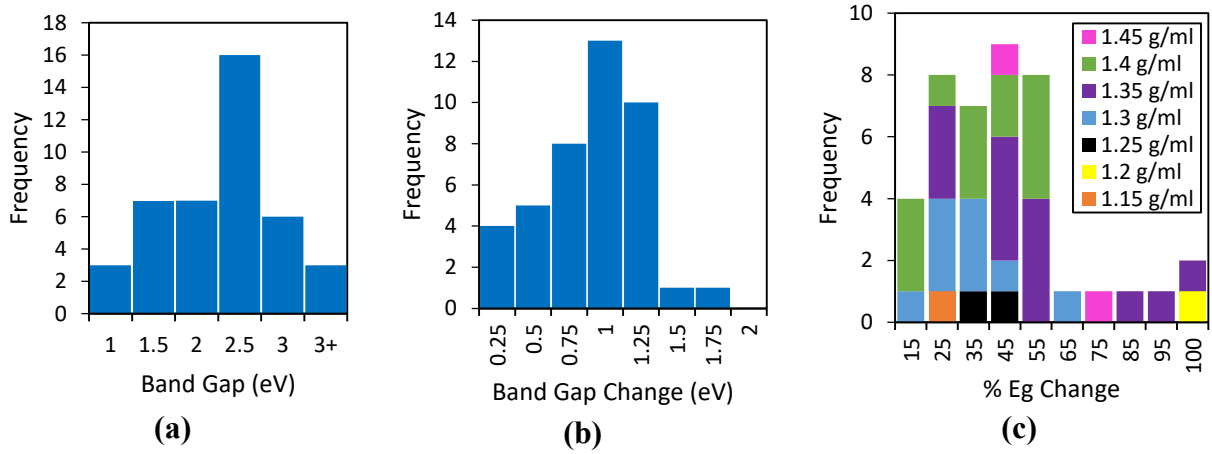


Figure 2. Ambient and pressure dependent E_g^{PBE} distributions for 42 HB-PAHs: (a) E_g^{PBE} distribution at ambient pressure; (b) Absolute change in E_g^{PBE} from 0-20 GPa; (c) Percent change in E_g^{PBE} from 0-20 GPa with respect to the density at 0 GPa. For TETCEN01, PENCEN, KEGHEJ01 and FANNUL E_g^{PBE} completely closes. This is a result of deficiencies in the PBE functional, as shown below and elsewhere¹⁷.

A continuous decrease in the PBE derived gaps (E_g^{PBE}) as a function of pressure is observed for most HB-PAHs studied here. Plots of E_g^{PBE} as a function of pressure for all structures are provided in **SI Fig S8**. Here, we only show representative examples. A typical

example is shown in **Fig. 1a** for the cruciform series. Similar pressure dependent narrowing of E_g has been reported for the oligoacenes¹⁷, the three polymorphs of rubrene, ²⁰ and picene¹⁶. For most HB-PAHs, the pressure dependent decrease in E_g^{PBE} is continuous, reinforcing the idea that few pressure induced phase transitions occur in this packing motif of PAHs at low temperature (this was also demonstrated in the accompanying pressure dependent structural study³⁶). A few structures exhibit discontinuous increases or decreases in the pressure dependent E_g^{PBE} plots, as seen in **Figs 1b & c**, hinting at the possibility of pressure induce phase transitions. These discontinuities are examined in detail in **section 3.1.7**.

The ambient pressure E_g^{PBE} distribution for all 42 HB-PAHs studied here is presented in **Fig** 2a. The average E_g^{PBE} and the STD of the distribution were found to be 2.08 eV and 0.73 eV, respectively. The most probable E_g^{PBE} -bin occurs in the 2 to 2.5 eV range with 37% of structures exhibiting gaps in this range. The smallest 0 GPa gap occurred for KAGGEG (0.76 eV) and the largest for BENZEN (4.36 eV). The absolute pressure dependent E_g^{PBE} -change distribution (from 0 to 20 GPa) is shown in **Fig 2b**. The average E_g^{PBE} -change and the STD of the distribution were found to be 0.86 eV and 0.42 eV, respectively. The most probable bin is in the 0.75 to 1 eV range with 31% of structures exhibiting this amount of change in their E_g^{PBE} . The smallest E_g^{PBE} -narrowing occurred for the pressure resistant structure of VEHCAM (0.22 eV change, or 10.54% of its 0 GPa value), while extreme pressure sensitivity was observed for FANNUL, which exhibited a E_g^{PBE} -narrowing of about twice the average at 1.62 eV.

The distribution in the percent change of E_g^{PBE} over the 20 GPa range is presented in **Fig 2c** for all structures. Here, the average percent change is observed to be ~37%, where the 35% to 45% bin is the most probable, containing 21% of structures. The STD of the distribution is 22%, and is attributed to the large deviations in intermolecular electronic couplings within the HB-PAHs (this manifests in the wide variety of intermolecular close contact fractions in the **SI** of Part 1³⁶). The three most and three least pressure sensitive crystal structures with respect to the percent change in E_g^{PBE} from 0 to 20 GPa are tabulated in **SI Table S2**. Surprisingly, there is little to no correlation between the density of the structure at 0 GPa and the pressure dependent gap narrowing, as seen in **Fig 2c**. Some correlation between the Hirshfeld-surface intermolecular close contact fractions present at 0 GPa and the pressure dependent gap narrowing were observed, as discussed in more detail in the **SI**. We note that for TETCEN01, PENCEN, KEGHEJ01, and FANNUL, the PBE gap drops to zero with increasing pressure. This can be attributed to the deficiencies of PBE and is addressed in the following subsections where we analyze trends within chemical families.

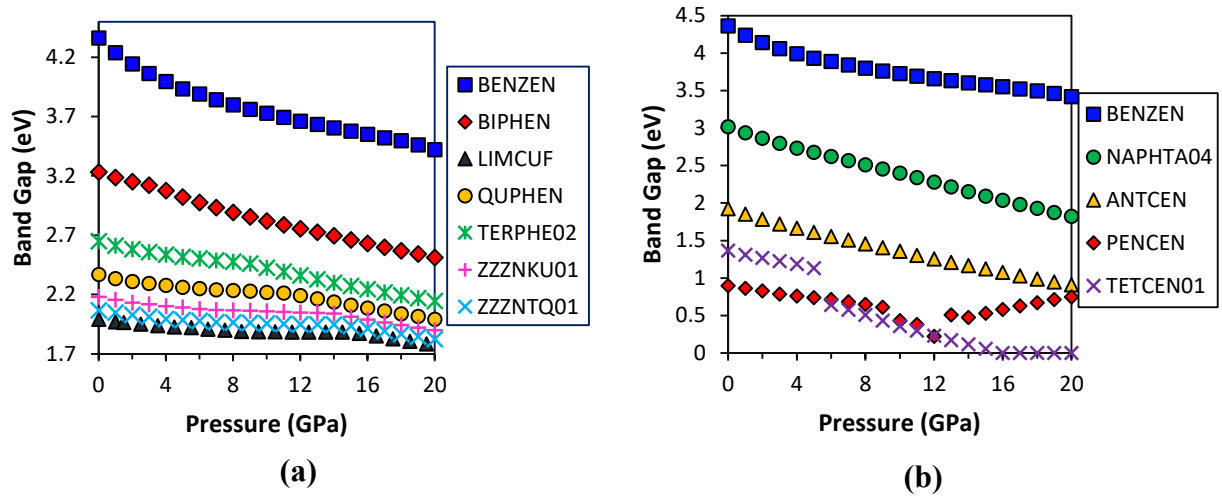


Figure 3. E_a^{PBE} as a function of pressure for (a) poly(*para*-phenylenes) and (b) oligoacenes.

3.1.2 E_g pressure dependence of poly(para-phenylenes) and oligoacenes: For all poly(para-phenylenes), the E_g^{PBE} decreases continuously with pressure as shown in Fig 3a. However, the E_g^{PBE} pressure dependence differs as the number of phenylene units increases. Specifically, the poly(para-phenylenes) with the largest gaps at ambient pressure have the strongest E_g^{PBE} pressure dependence; i.e., as the number of rings in the molecular units increases, the pressure dependent E_g^{PBE} -change decreases (from absolute and % standpoints). However, the structures with larger E_g^{PBE} at ambient pressure maintain larger E_g^{PBE} s over the entire 20 GPa range. To further demonstrate these trends, the 0 GPa E_g^{PBE} , absolute difference in E_g^{PBE} , and the percent difference in E_g^{PBE} from 0 to 20 GPa are provided in SI Table S4.

A somewhat different pressure dependent E_q^{PBE} behavior is found for the oligoacenes as shown in Fig 3b. As with the poly(para-phenylenes), the 0 GPa E_g^{PBE} decreases with increasing number of rings (see SI Fig S6 and SI Table S4). Likewise, the absolute change in E_g^{PBE} from 0-5 GPa decreases as the number of rings increases. However, the percent change in the E_a^{PBE} from 0-5 GPa increases with increasing number of rings for the oligoacenes (see SI Table S4). This is likely due to stronger intermolecular coupling, which manifests in a decrease in the amount of H···H interactions as the number of rings increases (see Fig 2 in Ref ¹⁷). A continuous E_a^{PBE} decrease is observed for benzene, naphthalene, and anthracene up to 20 GPa. However, tetracene undergoes a pressure induced phase transition around 6 GPa, which causes a discontinuous decrease in E_g^{PBE} , and pentacene exhibits an anomalous increase in E_g^{PBE} with pressure, which was also observed experimentally (these transitions are discussed in detail in Ref ¹⁷ and references therein). It is interesting to note that the oligoacenes always have a smaller E_a^{PBE} compared to the para(poly-phenylenes with same number of rings. This may be attributed to the seamless conjugation of the oligoacenes, whereas the conjugation is broken between phenylene units in the para(poly-phenylenes) because of ortho-hydrogen repulsion. The pressure dependent decrease in E_q^{PBE} is also always larger for the oligoacenes than poly(para-phenylenes) with the same number of rings from 0-5 GPa, as well as for oligoacenes with continuous E_a^{PBE} pressure dependence up to 20 GPa (detailed in SI Table S4).

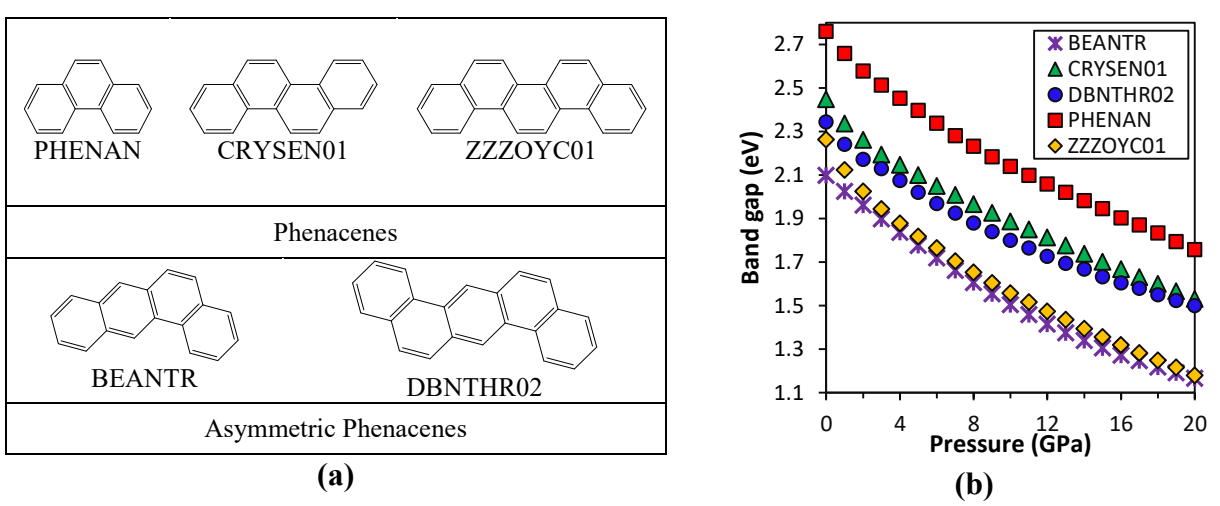


Figure 4. (a) Structures and CSD reference codes of phenacenes and asymmetric phenacenes. (b) Band gap as a function of pressure for phenacenes and antisymmetric phenacenes.

3.1.3. Phenacenes and Antisymmetric Phenacenes. The 0 GPa E_g^{PBE} decreases with increasing number of rings for the phenacenes as seen in **Fig 4**. However, the antisymmetric phenacenes exhibit an *increase* in the 0 GPa E_g^{PBE} with increasing number of rings. For both groups, E_g^{PBE} decreases continuously for all structures. For DBNTHR02 and ZZZOYC01, discontinuities are found in the unit cell parameters and intermolecular close contacts³⁶. However, these are not accompanied by discontinuities in E_g^{PBE} . This demonstrates that large structural changes are not always accompanied by significant changes in the electronic properties.

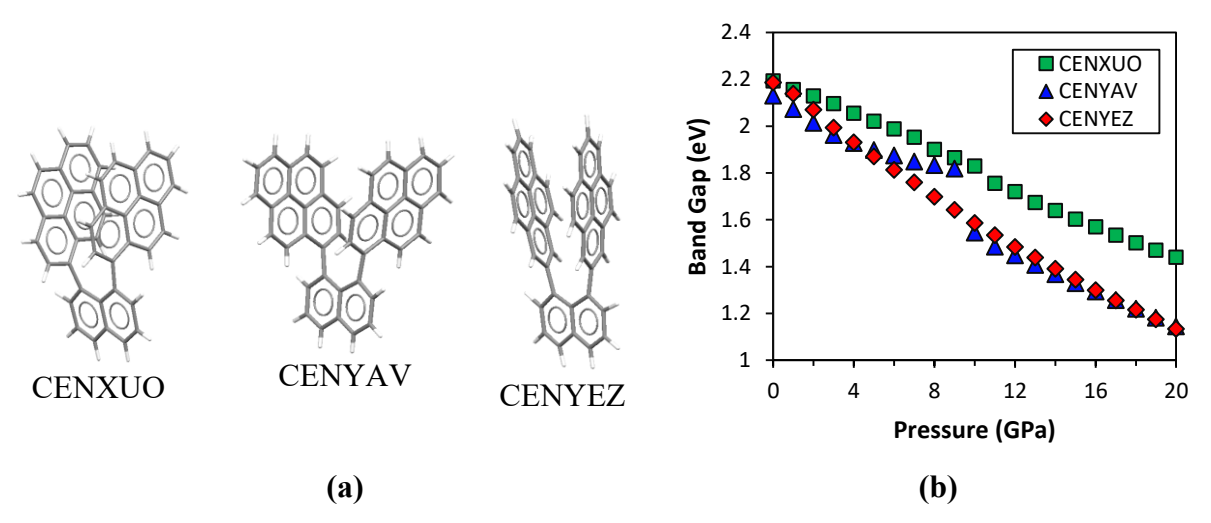


Figure 5. (a) Molecular structures and REF codes of the 1,8-dipyrenylnaphthalenes as extracted from the crystal structure at 0 GPa. (b) Band Gap as a function of pressure for 1,8-Dipyrenylnaphthalenes.

3.1.4. 1,8-Dipyrenylnaphthalenes. The three isomers of 1,8-Dipyrenylnaphthalene, shown in **Fig 5**, have a similar E_g^{PBE} at 0 GPa (varying by less than 60 meV), despite the significant differences in their unit cell parameters and intermolecular close contact fractions, reported in Part 1^{36} . However, each system exhibits a unique E_g^{PBE} pressure dependence, which correlates

with the structural pressure dependence observed in Part 1^{36} . CENYEZ shows a continuous decrease in E_g^{PBE} over the 20 GPa range. Its structural isomer, CENXUO (see **Fig 5**) has a nearly continuous E_g^{PBE} pressure dependence, except for a small discontinuity between 10 and 11 GPa, consistent with the structural rearrangements observed in **Figs 23** & **24** of Part 1^{36} . The stereoisomer of CENXUO, CENYAV, shows an exponential decrease in E_g^{PBE} up to 9 GPa, at which point the large structural rearrangements reported in Part 1^{36} cause a significant modification of the electronic properties, resulting in a discontinuity between 9 and 10 GPa. Above 10 GPa, the E_g^{PBE} decreases continuously with pressure. The discontinuities in the E_g^{PBE} pressure dependence are discussed further in **section 3.1.7**.

3.1.5. Aryl Oligoacene Derivatives (Cruciforms). For the aryl oligoacene derivatives, shown in Fig. 6, the 0 GPa E_g^{PBE} decreases with increasing number of rings, as shown in Fig 1a, although the difference between QQQCIG04 and VEBJES is small (40 meV). This may be attributed to poor intermolecular electronic coupling in the VEBJES crystal, as single molecule calculations show that the HOMO-LUMO gap (E_g^{H-L}) of VEBJES is 0.41 eV smaller than that of QQQCIG04.³⁹ In the solid state, the energy gap of QQQCIG04 shrinks by 0.44 eV, whereas that of VEBJES shrinks by only 0.07 eV (indicating significantly less dispersed bands). The E_g^{PBE} of the aryl oligoacene derivatives decreases continuously over the 20 GPa range, as shown in Fig 1a. The pressure induced gap narrowing of DPANTR01 ($\Delta E_g^{PBE} = 0.54$ eV) and QQQCIG04 ($\Delta E_g^{PBE} = 0.91$ eV) is stronger than that of VEBJES ($\Delta E_g^{PBE} = 0.32$ eV). The weaker pressure response of VEBJES may be attributed to the nearly flat pressure dependence of the H···H intermolecular close contacts and the *negative* pressure dependence of the C···H intermolecular close contacts as seen in Figs 7 & 9 of Part 1³⁶. This leads to poor coupling between the HOMOs and LUMOs of neighboring molecules, as H···H interactions generate repulsion and prevent molecules from getting closer to one another in a preferential manner for frontier orbital overlap.

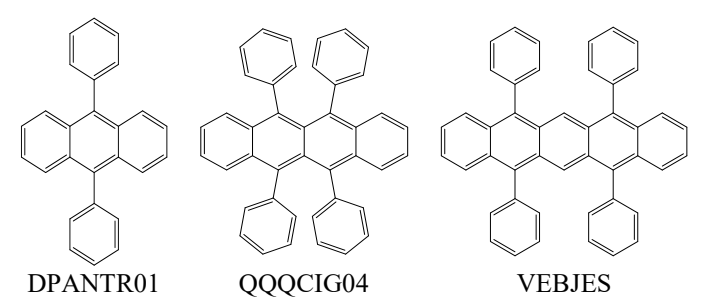


Figure 6. Structures and pressure dependent E_g^{PBE} plot for phenylated acenes (cruciforms)

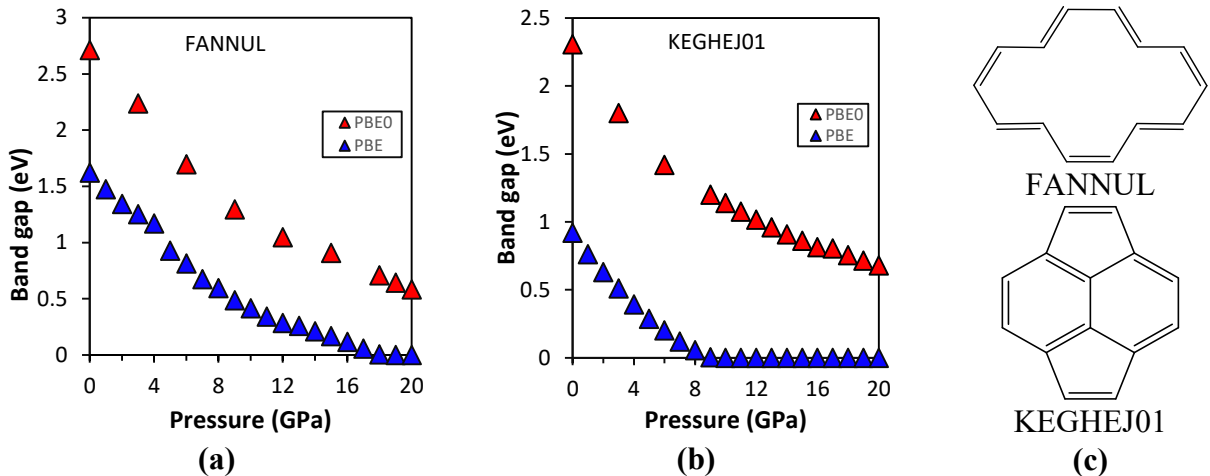


Figure 7. Band gap as function of pressure as calculated with PBE and PBE0 for (a) annulene[14] (FANNUL) and (b) pyracylene.(KEGHEJ01) (c) Structure of KEGHEJ01 and FANNUL at ambient pressure.

3.1.6 Unique E_g pressure dependence of pyracylene and annulene[14]: Pyracylene (KEGHEJ01) is unique among the PAHs studied here because it contains two aromatic five membered rings attached to a naphthalene core (see Fig 7c). Its orthorhombic unit cell contains 6 molecules (Z=6) in a HB configuration and has a Cmca space group. SAnnulene[14] (FANNUL) is unique because it is continuously aromatic over 14 carbon atoms, as opposed to be comprised of six-membered aromatic rings (see Fig 7c). The monoclinic unit cell of FANNUL has a P2₁/c space group with Z=2. Set E_g^{PBE} as a function of pressure up to 20 GPa is plotted for FANNUL and KEGHEJ01 in Figs 7a & b, respectively. E_g^{PBE} of FANNUL and KEGHEJ01 goes to zero for pressures above 17 GPa and 9 GP, respectively. Because PBE is known to underestimate E_g in PAHs, PBE0 was used to confirm the pressure dependence of E_g using the optimized PBE+vdW structures, following the procedure we have established for tetracene and pentacene PBE+vdW structures, following the procedure we have established for tetracene and pentacene PBE+vdW structures, following the procedure we have established for tetracene and pentacene PBE+vdW structures shows a steady decrease over the 20 GPa pressure range. Our recommended best practice is to always use PBE0 (or another hybrid functional) for verification when PBE produces a zero gap.

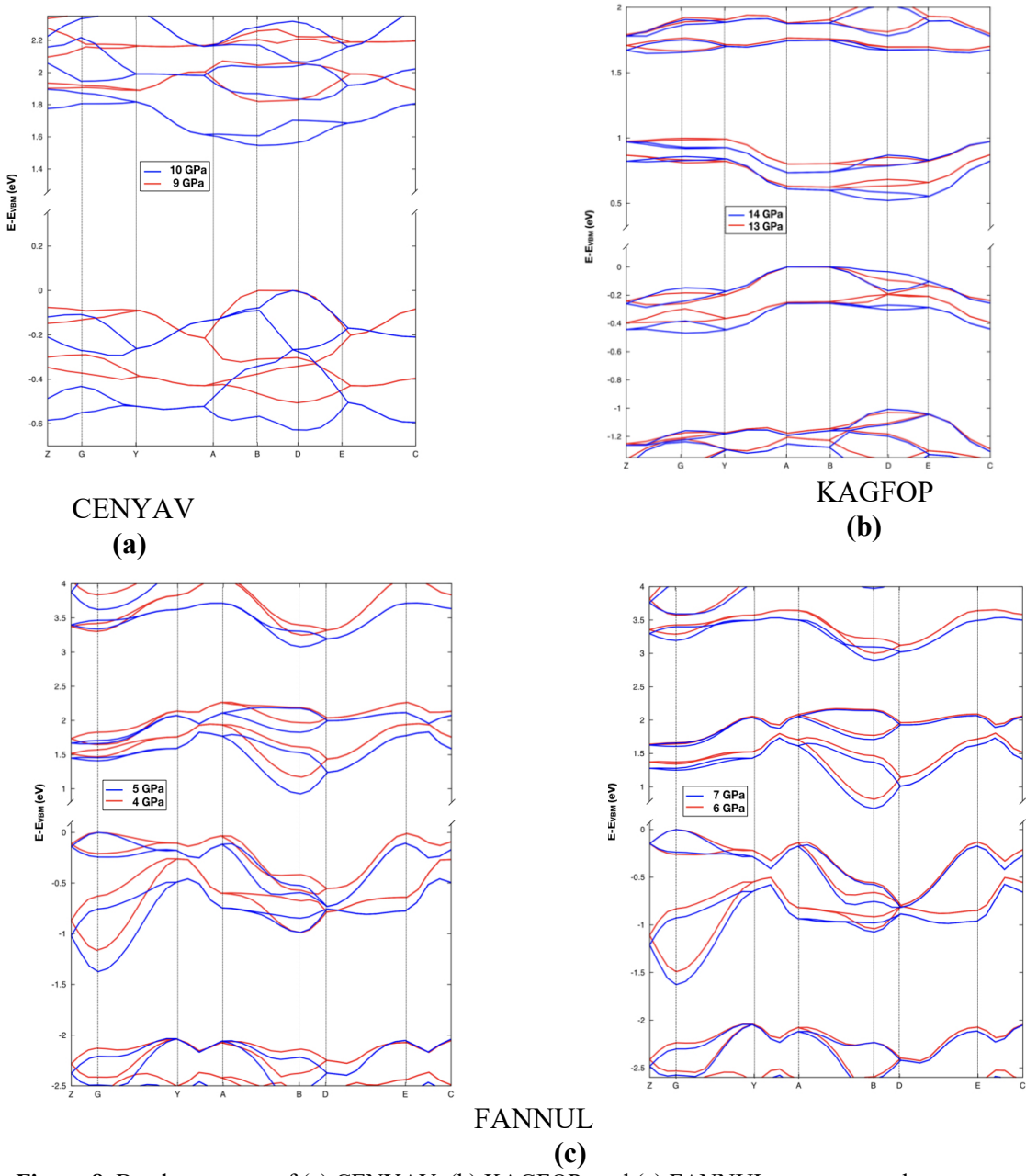


Figure 8. Band structures of (a) CENYAV, (b) KAGFOP, and (c) FANNUL at pressures that correspond to discontinuities in E_q^{PBE} pressure dependence. The top of the valance band is set to 0 eV.

3.1.7 Discontinuous Pressure Dependent Changes in E_g^{PBE} : The E_g^{PBE} vs. pressure plots for CENYAV, FANNUL, and KAGFOP exhibit discontinuous decreases in E_g^{PBE} with increasing pressure, as shown in Fig 1c. These discontinuities may be attributed to a combination of conformational and crystalline rearrangements. The largest single E_g^{PBE} discontinuous decrease of 0.27 eV is observed for CENYAV between 9 to 10 GPa. About half of this gap decrease can be attributed to increased intermolecular electronic coupling of the HOMO and LUMO, as indicated by the increase in the band dispersion by 0.043 eV for the HOMO-derived valence band and by 0.086 eV for the LUMO-derived conduction band, seen in Figs 8a & 9a. Fig 9a shows that the E_g^{PBE} discontinuity is accompanied by a discontinuous increase in the band

dispersion with respect to pressure for both frontier orbitals. The remaining energetic differences may be explained by the conformational change of the molecule, shown in **Fig 10a**. The naphthalene and pyrene moieties become twisted (bent), which may reduce the aromatic stabilization energy. Consequently, the band origins become closer in energy, further reducing E_q^{PBE} as seen in **Fig 8a**.

A discontinuous 0.1 eV decrease in E_g^{PBE} of KAGFOP is observed between 13 to 14 GPa in **Fig 1c**. Again, the narrowing of the gap is attributed to increased band dispersion, combined with a change of molecular conformation. The dispersion increases by 0.010 eV for the HOMO and by 0.069 eV for the LUMO as seen in **Figs 8b** and **9b**. Only the larger change in the LUMO bandwidth is observed as a discontinuity in **Fig 9b**. Single point energy calculations performed on the molecular units as extracted from the crystals at 13 and 14 GPa show that the minor perturbations of the phenyl side groups (see **Fig 10b**) modulate the band origin energies, lowering the LUMO and raising the HOMO, accounting for the remaining energetic difference (see **SI Table S11** for single point energy results).

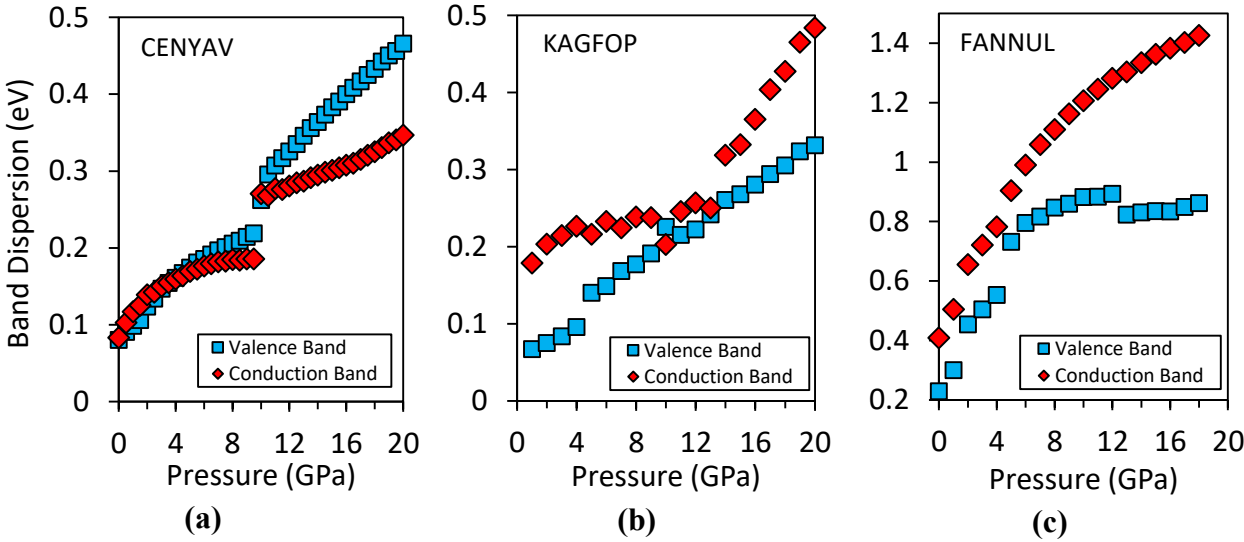


Figure 9. Dispersion of the HOMO-derived valence band and the LUMO-derived conduction band as a function of pressure for (a) CEYAV, (b) KAGFOP and (c) FANNUL.

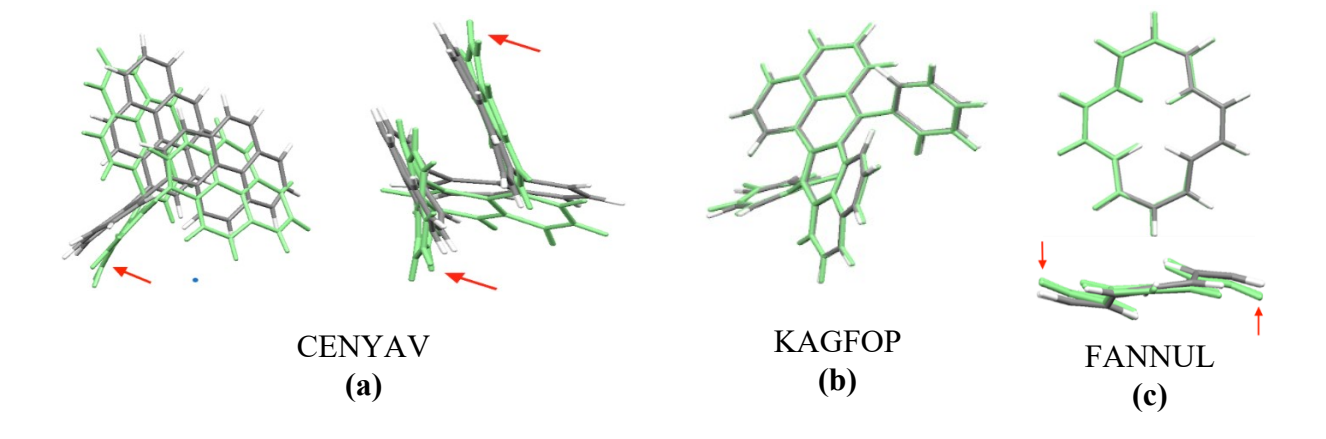


Figure 10. Change in the conformation of a molecule extracted from the crystal structures of (a) CENYAV side and face views at 9 and 10 GPa, (b) KAGFOP at 13 and 14 GPa, and (c) FANNUL side and face on views at 4 and 5 GPa. Light green structures corresponds to higher pressure.

 E_g^{PBE} of FANNUL exhibits a discontinuous decrease of 0.24 eV between 4 and 5 GPa and another of 0.14 eV between 6 and 7 GPa, as shown in **Fig 1c**. The first discontinuity is associated with increases of 0.18 eV in the dispersion of the HOMO-band and 0.12 eV for the LUMO-band, as evident in **Figs 8c** and **9c**. Single point energy calculations of the molecules as extracted from the crystal structures at 4 and 5 GPa show a shift of the band origin energies due to changes in the molecular conformation, as illustrated in **Fig 10c**. This slightly broadens the HOMO-LUMO gap by 0.03 eV. The net effect of the large dispersion increase and the small molecular gap broadening leads to a net narrowing of the crystal band gap. The second discontinuity at 6-7 GPa is accompanied by a 0.021 eV increase in the dispersion of the HOMO-band and 0.069 eV increase for the LUMO-band. The remainder of the energy difference is attributed to further conformational reorganization of the molecules, resulting in a downward shift of the LUMO band as seen in **Fig 8c**. Notably, the larger discontinuity in E_g^{PBE} at 4-5 GPa is accompanied by a significant discontinuous increase in the band dispersion, whereas the smaller discontinuity at 6-7 GPa E_g^{PBE} corresponds to a nearly continuous increase in the band dispersion.

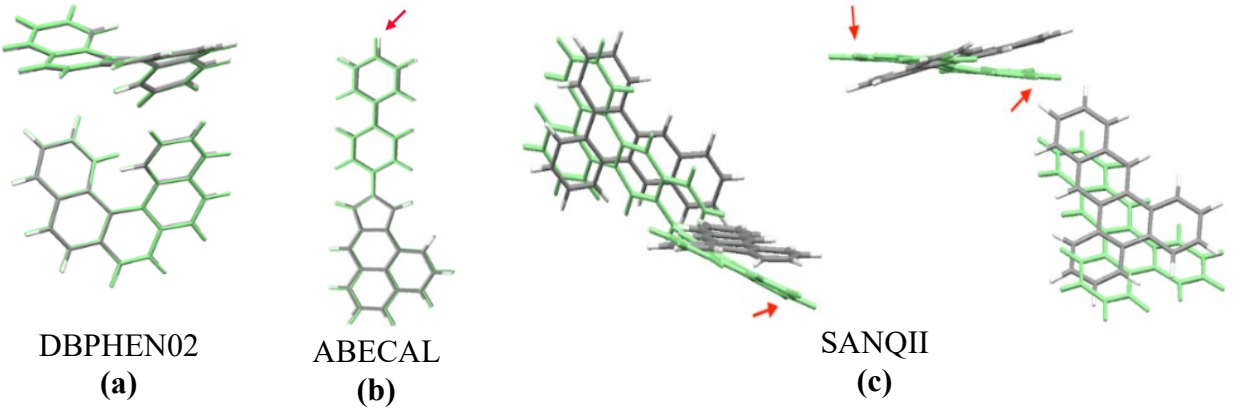
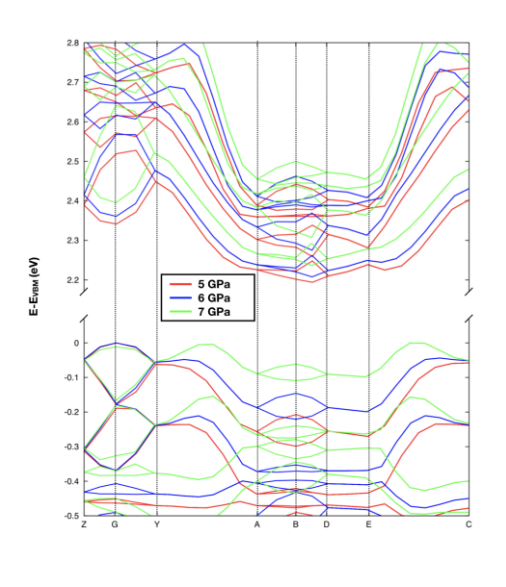


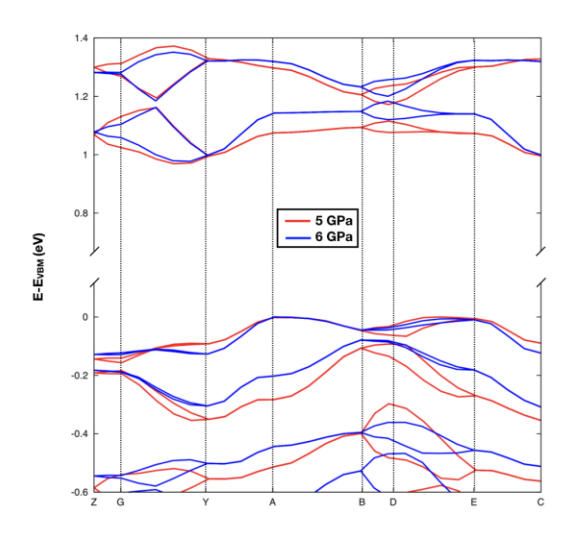
Figure 11. Conformational changes in molecules extracted from the crystal structures of (a) DBPHEN02 at 6 and 7 GPa, side view on top and face view on the bottom; (b) ABECAL at 5 and 6 GPa; and (c) two views of the two inequivalent molecules of SANQII at 7 and 8 GPa as orientated in the crystal. The light green structures correspond to higher pressures.

Fig. 1b shows the pressure dependence of E_g^{PBE} for ABECAL, DBPHEN02, and SANQII. In contrast to the pressure dependent E_g^{PBE} decreases presented in **Fig 1c**, all three structures exhibit some pressure dependent E_g^{PBE} increases. For DBPHEN02, a 0.014 eV increase is observed between 5 to 6 GPa, with another 0.029 eV increase occurring between 6 to 7 GPa. An overlay of the molecular structure of DBPHEN02 at 6 and 7 GPa as extracted from the crystal structure is shown in **Fig 11a**, and demonstrates little perturbation of the molecular structure with increased pressure. However the HOMO-LUMO gaps of the molecules as extracted from the crystal at 4, 5, and 6 GPa broaden with increasing pressure (see **SI Table S11**). Therefore, the increase in E_g^{PBE} is a result of changes in the electronic coupling of the frontier MOs and the band origin energies. **Fig 12a** shows that the bottom of the conduction band

sequentially shifts to higher energy with increasing pressure, broadening E_g^{PBE} . Based on the band structures of DBPHEN02 in **Fig 12a**, and the band dispersion vs pressure plots in **Fig 13a**, the dispersion of the HOMO-band is observed to decrease about sevenfold more than the LUMO band dispersion increases from 5 to 6 GPa. From 6 to 7 GPa the HOMO-band dispersion further decreases about tenfold more than the LUMO-band dispersion increases. The decreased valence band dispersion above 5 GPa indicates that the electronic coupling between the HOMOs of neighboring molecules is decreasing, whereas the LUMO coupling is increasing.

For ABECAL, a discontinuous increase of 0.024 eV in E_g^{PBE} is observed from 5 to 6 GPa. **Figs 12b** and **13b** show that, in contrast to the dispersion trends of DBPHEN02, the dispersion of the LUMO band of ABECAL increases about 2.5 times more than the HOMO band dispersion decreases from 5 to 6 GPa. Based on the net increase in the band dispersion, one would expect E_g^{PBE} to decrease. However, the molecular units distort under pressure, as indicated by red arrows in **Fig 11b**. This causes an increase in the HOMO-LUMO gap as determined *via* single point calculations on molecules extracted from the crystal structures at 5 and 6 GPa, which leads to broadening of E_g^{PBE} (see **SI Table S11**). Therefore, the increase in E_g^{PBE} is attributed predominantly to changes in the band origin energies, associated with the molecular geometry.





DBPHEN02 (a)

ABECAL (b)

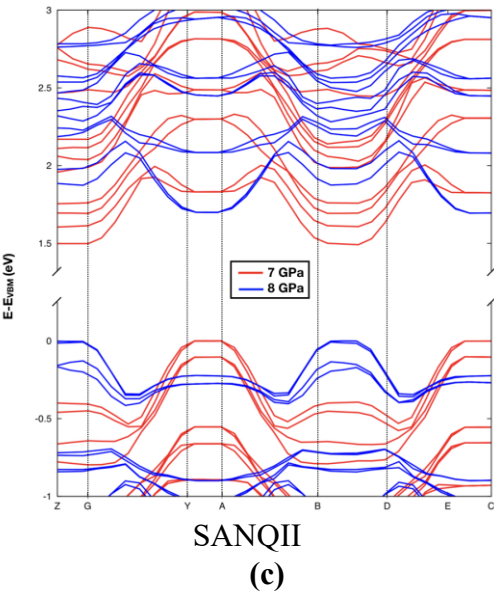


Figure 12. Band structures of DBPHEN02, ABECAL, and SANQII at pressures that correspond to discontinuities in E_g^{PBE} . The top of the valance band is set at 0 eV.

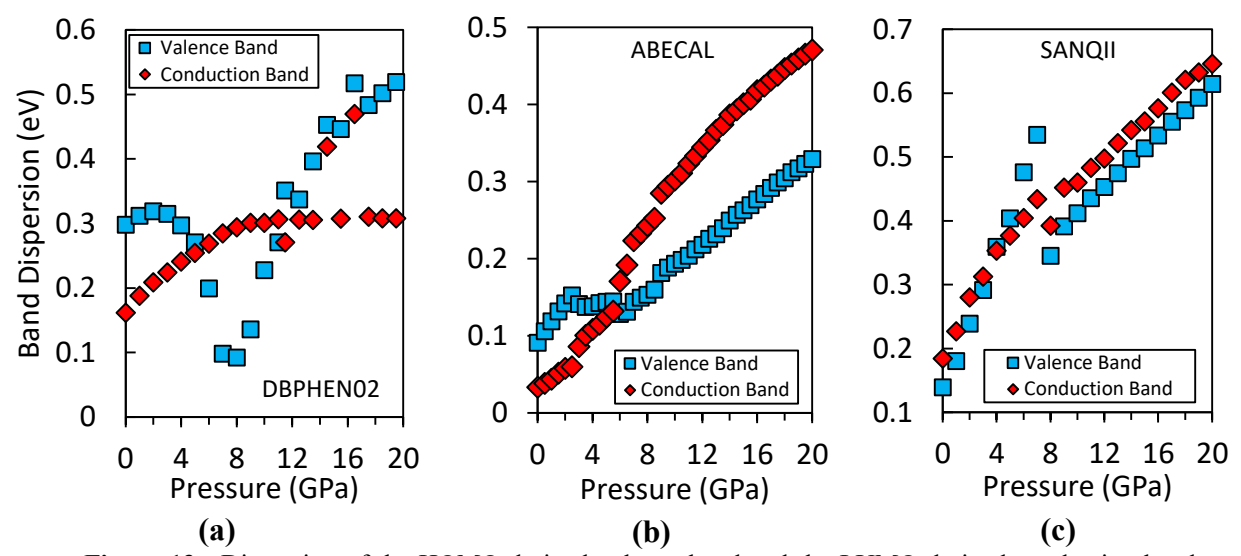


Figure 13. Dispersion of the HOMO-derived valence band and the LUMO-derived conduction band as a function of pressure for a) DBPHEN02, b) ABECAL and c) SANQII.

For SANQII, there is a discontinuous 0.2 eV increase in E_g^{PBE} from 7 to 8 GPa in **Fig 1b**. An overlay of the structures of the two inequivalent molecules in the unit cell of SANQII at 7 and 8 GPa shows significant perturbation of the molecular arrangement within the crystal, as indicated by red arrows in **Fig 11c**. Additional pressure dependent deformations not seen here are shown in **SI Fig S3**). In SANQII, the dispersion of the HOMO band decreases by 0.014 eV from 7 to 8 GPa and the dispersion of the LUMO band decreases by 0.19 eV, as shown in **Figs 12c** and **13c**. However, single point calculations for molecules extracted from the crystal structures show that the HOMO-LUMO gap at 8 GPa is smaller than at 7 GPa. Therefore, the net increase in E_g^{PBE} is primarily the result of changes in the electronic coupling of the frontier molecular orbitals.

3.2. Pressure-Induced Direct/Indirect E_g Transitions: Semiconductors may exhibit either direct or indirect band gap. In direct semiconductors, the top of the valance band and the bottom of the conduction band are at the same k-point, such that creating an electron-hole pair (exciton) only requires a photon with sufficient energy to vertically excite an electron across the gap. For indirect semiconductors, the top of the valance band and the bottom of the conduction band are at different k-points, such that exciting an electron across the gap requires coupling to a phonon transition to satisfy momentum conservation.⁵⁷ As a result, the rate of exciton creation in indirect semiconductors is slower than in direct semiconductors. Therefore, a direct gap is more desirable for optoelectronics applications, whereas those with an indirect E_g are good for microelectronics applications.⁵⁷⁻⁶⁰

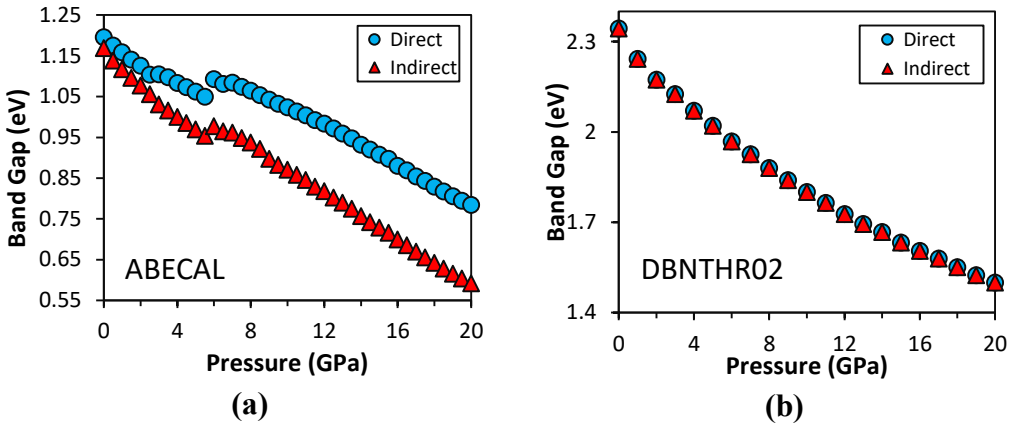


Figure 14. Smallest direct and indirect band gaps as a function of pressure for (a) ABECAL and (b) DBNTHR02.

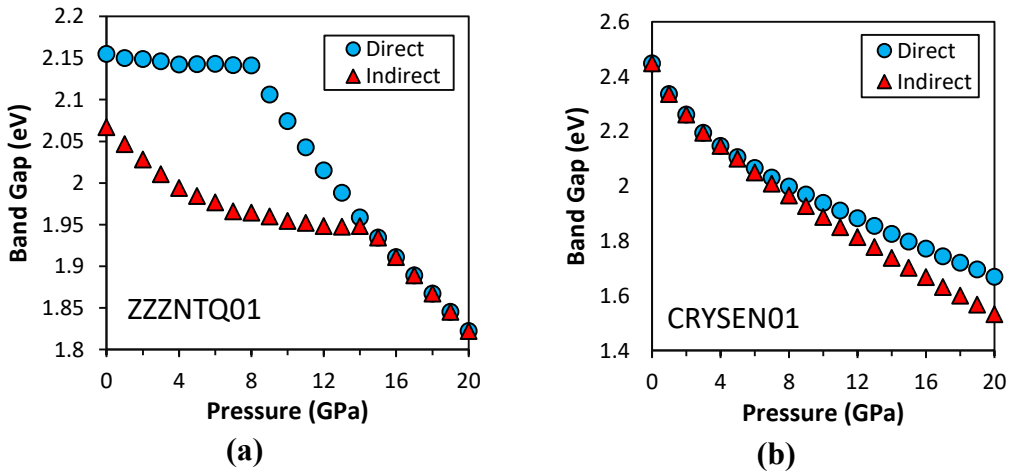


Figure 15 Direct/indirect switching of E_g in PAHs under pressure: (a) E_g changes from indirect to direct for ZZZNTQ01; (b) E_g changes from direct to indirect for CRYSEN01.

To show the effect of pressure on whether the band gap is direct or indirect, the smallest direct and indirect E_g values are plotted as a function of pressure for all structures in **SI Fig S9**. The lower value of the two at any given pressure determines whether the material is a direct or indirect semiconductor (if the direct and indirect values are the same, it is considered direct). For

most HB-PAHs, E_g remains direct or indirect over the entire pressure range. Representative examples for the indirect E_g of ABECAL and the direct E_g of DBNTHR02 are shown in **Fig. 14**. In contrast, some PAHs exhibit a direct/indirect transition upon pressurization. For instance, ZZZNTQ01 has an indirect E_g from 0 GPa to 14 GPa, at which point it switches to a direct E_g , as shown in **Fig 15**. CRYSEN01 undergoes the opposite transition from a direct E_g up to about 3.5 GPa to an indirect E_g for pressures up to 20 GPa. This may be attributed to changes the MO coupling and the resulting band structure under pressure, as shown in **Fig. 16**.

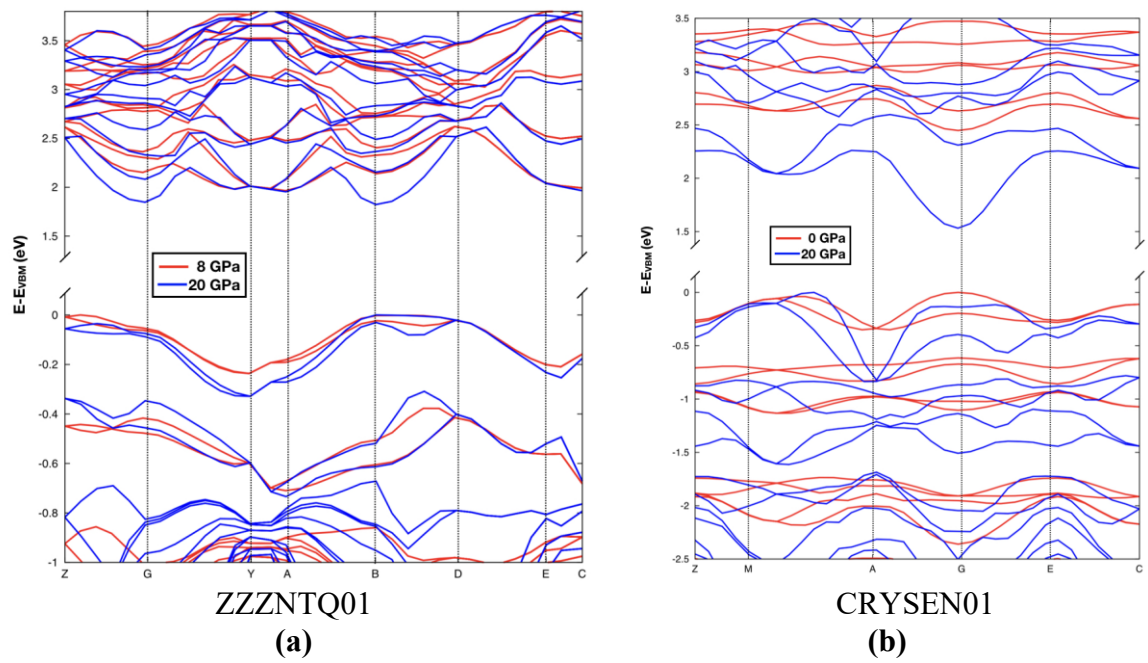


Figure 16: Band structure of (a) ZZZNTQ01 at 8 and 20 GPa, and (b) CRYSEN01 at 0 and 20 GPa.

3.3. Pressure Dependence of Band dispersion

Pressure-Induced Polarity Switching: Organic optoelectronic devices require organic semiconductors with high carrier mobilities. Transport in organic semiconductors may occur via hopping, whereby localized charge carriers move from one site to the next, overcoming an activation barrier. This mechanism is typical of weakly coupled or disordered materials. In strongly coupled crystalline materials, the dominant mechanism is typically band transport, whereby delocalized carriers have an effective mass, which is inversely proportional to the band curvature. Transport in organic semiconductors may also occur in an intermediate regime between the limiting cases of hopping and band transport. ^{61,62} Here, we focus on the band transport regime in crystalline HB-PAHs. In this regime, the hole and electron mobilities are related to the width and curvature of the valence and conduction bands, respectively. 63 The larger the band dispersion of the valence (conduction) band, the higher the hole (electron) mobility. The bandwidth (band dispersion) is defined as the energy difference between the high and low energy limits of a particular band. The widths of the HOMO-derived highest energy valence band and the LUMO-derived lowest energy conduction band correspond to the hole and electron mobilities, respectively. An organic semiconductor is considered to be in the band transport regime if its bandwidth is at least 0.1 eV.⁶⁴ The band dispersion is associated with the strength of the electronic coupling between similar molecular orbitals of neighboring molecules.^{52,64–68,62}

Therefore, changes in the distances and relative orientation between molecules can be used to tune the band dispersion^{50,52}, and pressure is the perfect tool for exploring these effects. Relevant examples of the use of hydrostatic-pressure leading to increased conductivity in HB-PAHS can be seen for single crystal pentacene and tetracene,²² pentacene thin-films,⁶⁹ and single crystal rubrene⁷⁰.

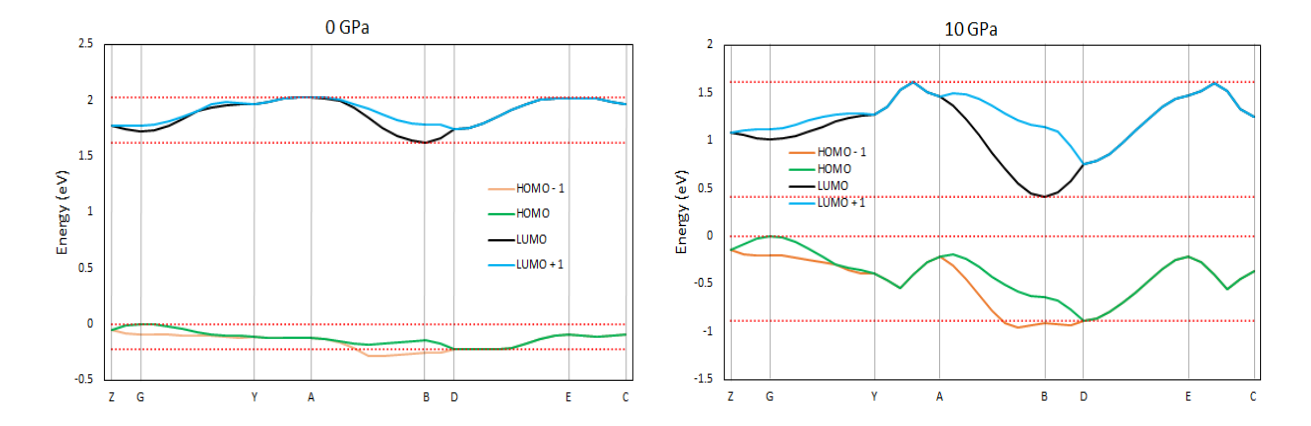


Figure 17. Band structure of FANNUL at 0 and 10 GPa. The top two bands of the valence band and the bottom two of the conduction band demonstrate the general effect of pressure on band dispersion. Dotted red lines are tangents to the minimum and maximum of the highest energy valence band (green band) and lowest energy conduction band (black band). Note the general shift of the conduction band closer to the Fermi level (0 GPa) under pressure.

As reported in Part 1 of this study, ³⁶ the intermolecular distances in crystalline HB-PAHs typically decrease under pressure and the relative orientations change, such that co-facial and face-to-edge intermolecular interactions increase while edge-to-edge contacts decrease. Therefore, pressurization typically leads to stronger electronic coupling between the frontier orbitals of neighboring molecules, which results in increased band dispersion. Fig 17 presents an example of the band structure of FANNUL at 0 GPa and 10 GPa, showing that the top of the valence band and bottom of the conduction band become more dispersed (broader) with pressure due to increased frontier orbital overlap. Fig 18 shows the probability distributions of the HOMO and LUMO band dispersion for the HB-PAHs at 0 GPa and at the pressure where the dispersion is maximal (typically 20 GPa). The average value for the dispersion of the HOMOderived valence and LUMO-derived conduction bands at 0 GPa was found to be 0.20 eV and 0.25 eV with a standard deviation of 0.16 eV and 0.21 eV, respectively. The outliers with particularly high bandwidths are the low temperature metastable HB structure of perylene (PERLEN07), and pyracylene (KEGHEJ01). The average value for the maximum dispersion across the entire pressure range was found to be 0.61 eV for the valence band and 0.60 eV for the conduction band, with standard deviations of 0.35 eV and 0.29 eV, respectively. Structures displaying the largest high pressure dispersion are FANNUL and again PERLEN07. Refcodes and corresponding values used to construct Fig 18 are available in SI Table S7.

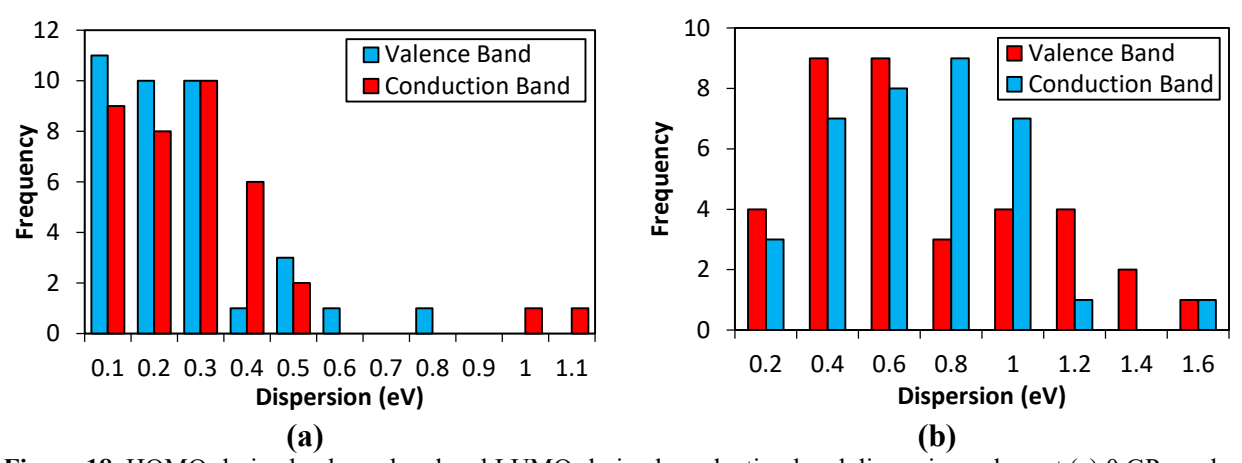


Figure 18. HOMO-derived valence band and LUMO-derived conduction band dispersion values at (a) 0 GPa and (b) maximum dispersion values within the pressure series. In **a**, outlying structures with VB in 0.7-0.8 eV bin and CB in 0.9-1 eV bin is PERLEN07, CB in 1-1.1 eV bin is KEGHEJ01. In **b**, outlying structures in the 1.4-1.6 eV bin are PERLEN07 (VB) and FANNUL (CB).

The polarity of an organic semiconductor is determined by the relative bandwidths of the HOMO-derived valence band and the LUMO-derived conduction band. If the dispersion of bottom of the conduction band is greater than the top of the valence band the crystal will be an n-type semiconductor. If the opposite is true, the material will be a p-type semiconductor (where the majority of charge carriers in n-type semiconductors are electrons, and in p-type are holes). If the dispersion of the two bands is comparable (within ~ 0.015 eV), the material may be considered ambipolar. While most energy bands become more dispersed with increasing pressure for HB-PAHs, the widths of the valence and conduction bands may change at different rates, as summarized in **SI Fig S7** and **SI Table S5**. In many instances, the relative widths of the valence and conduction bands maintains a constant relationship, where one is greater over the entire pressure range and the polarity of the material remains fixed. However, some of the HB-PAHs exhibit polarity switching through ambipolar regions between regions of p-type and n-type behavior (and vice versa). For example, **Fig 13** shows polarity switching and ambipolar regions in DBPHEN02, ABECAL, and SANQII. We proceed to discuss the pressure dependence of the band dispersion and polarity for several families of HB-PAHs.

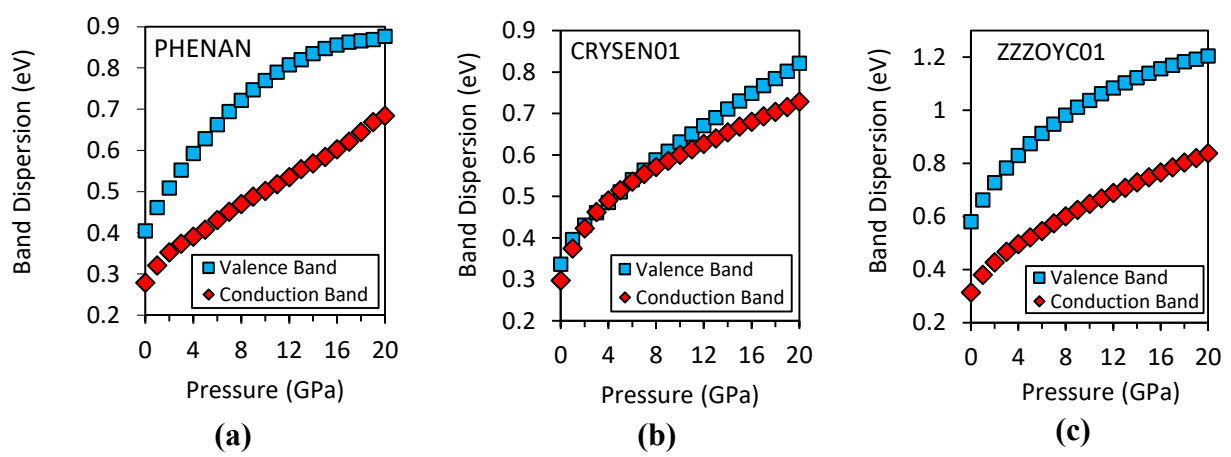


Figure 19. Bandwidth as a function of pressure for phenacenes: (a) phenenthrene, (b) chrysene, and (c) picene.

3.3.2. Phenacenes: Fig 19 shows the pressure dependence of the band dispersion of the phenacenes, phenanthrene (PHENAN), chrysene (CHRYSEN01), and picene (ZZZOYC01). All phenacenes exhibit a steady increase in the bandwidth as the pressure increases. For phenanthrene, the valence band is more dispersed than the conduction band at any pressure, implying p-type semiconductivity, where the majority of carriers are holes. This agrees well with previous theoretical work, where phenenathrene was shown to behave as a p-type semiconductor up to 30 GPa, reaching the amorphous silicon drift mobility for pressure above 9.3 GPa. Chrysene is a p-type semiconductor at ambient pressure, up to 2 GPa, where it becomes ambipolar as the valence and conduction bandwidths become approximately equivalent. These findings are consistent with a previous pressure dependent theoretical study, in which chrysene was found to become ambipolar at \sim 1.5 GPa. Here, we find that when the applied pressure exceeds 6 GPa, chrysene reverts to a p-type semiconductor. This is in contrast to Ref. 26 , where chrysene was predicted to become n-type above \sim 3 GPa. This discrepancy is most likely because a dispersion correction was not employed in Ref. 26 . Picene, like phananthrene, is predict to remain a p-type semiconductor throughout the 20 GPa pressure range.

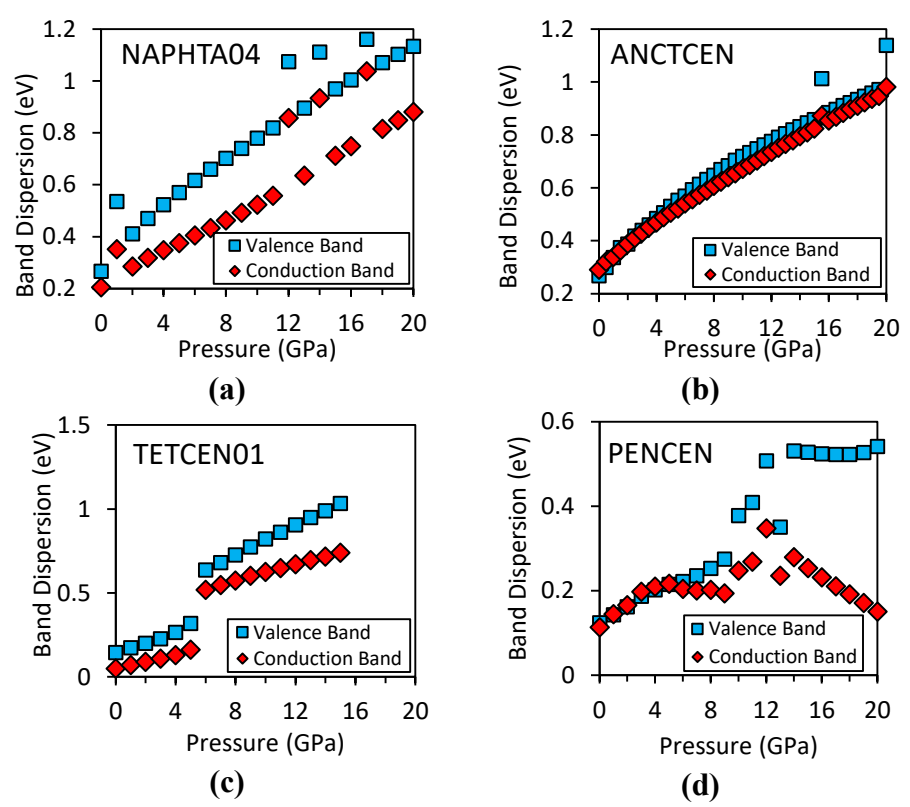


Figure 20. Bandwidth as a function of pressure for the oligoacenes: (a) naphthalene, (b) anthracene, (c) tetracene, and (d) pentacene. For tetracene, band dispersion above 16 GPa is not included because the PBE band gap goes to zero.

3.3.3. Oligoacenes: Fig 20 shows the pressure dependence of the band dispersion of the oligoacenes, naphthalene (NAPHTA04), anthracene (ANTCEN), tetracene (TETCEN01), and pentacene (PENCEN). Naphthalene and tetracene are found to be *p*-type semiconductors over the entire 20 GPa pressure range, despite exhibiting some discontinuities in the band dispersion. For TETCEN01, the discontinuity is associated with the experimentally observed phase transition occurring at 6 GPa. Anthracene is found to be *n*-type from ambient pressure to 1 GPa,

ambipolar from 1.5 GPa to 3.5 GPa, and *p*-type from 4 GPa to 20 GPa. However, the largest difference between the conduction and valence bandwidth in the *n*- and *p*-type regimes of anthracene is only on the order of 0.05 eV, making it nearly ambipolar over the entire 20 GPa range, in agreement with Ref. 19. Pentacene is arguably ambipolar at ambient pressure, as its valence band is only slightly broader than the conduction band by 0.011 eV and remains ambipolar up to 5 GPa. Above 5 GPa, pentacene is predicted to be *p*-type. A detailed comparison to previous theoretical work^{52,71} on the oligoacenes is provided in the **SI**.

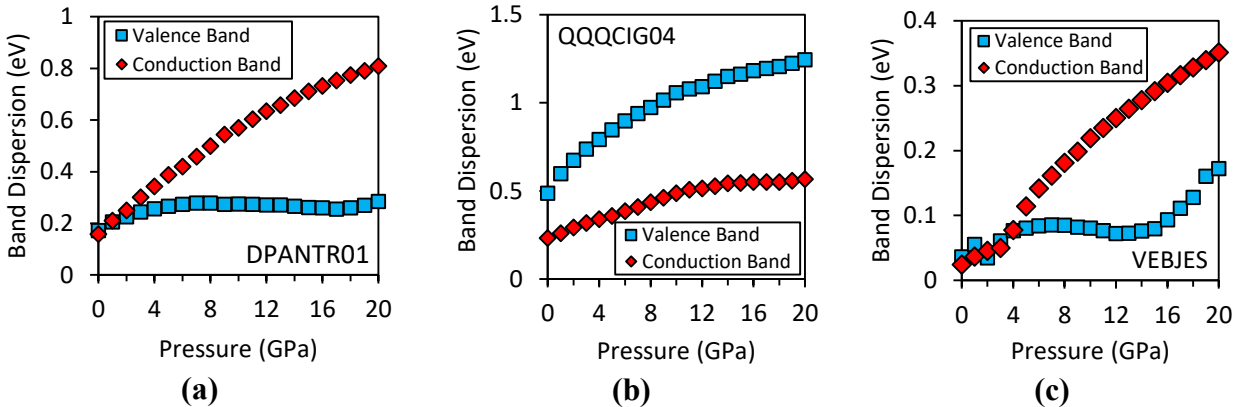


Figure 21. Bandwidth as a function of pressure for (a) DPANTR01, (b) QQQCIG04, and (c) VEBJES.

3.3.4. Cruciforms: Fig 21 shows the pressure dependence of the band dispersion of the cruciforms, whose molecular structures are shown in Fig 6. Both DPANTR01 and VEBJES have ambipolar regions at low pressures and switch to *n*-type polarities above ~ 5 GPa, whereas rubrene (QQQGIG04) maintains *p*-type polarity over the entire pressure range. Rubrene is known to possess a very high hole carrier mobility, reaching $\mu = 40 \text{ cm}^2/\text{V.s.}^{26}$ At ambient pressure, the bandwidths of its conduction band and valence band are 0.23 eV and 0.49 eV, respectively. This is in good agreement with previous work where values of 0.18 eV and 0.42 eV, respectively, were reported. The bandwidth of both the valence band and the conduction band increases monotonously with pressure, and at 20 GPa it is higher by a factor of 2-2.5 than at ambient pressure. Consequently, the carrier mobility is expected to strongly increase with increasing pressure, in agreement with the experimental observation that the conductivity of single crystal rubrene increases by a factor of 2.1 under pressure of 0.43 GPa.⁷²

3.3.5. Poly(para-phenylenes): The bandwidth of all poly(para-phenylenes), exhibits a similar pressure response, as shown in Fig 22. The valence bandwidth undergoes a continuous exponential increase throughout the entire pressure range. The conduction bandwidth shows an initial increase, followed a plateau region, followed by another increase up to 20 GPa. With increasing number of rings, the valence bandwidth approaches the asymptotic limit more slowly and the plateau region of the conduction bandwidth shifts to higher pressures. Most poly(para-phenylene) structures are *n*-type semiconductors across the entire pressure range, as shown in Fig 22 and SI Tables S3 & S5. Benzene (BENZEN) is ambipolar from 0 GPa to 7 GPa and converts to *n*-type above 7 GPa. Biphenyl (BIPHEN) is *n*-type at 0 GPa and alternates between ambipolar and *n*-type from ~2.5 to 13 GPa. This unique behavior is attributed to oscillations of the two phenyl rings with respect to one another, which in turn produces discontinuous changes in the pressure dependent intermolecular close contacts (see Fig 15 in Part 1³⁶) and MO overlap.

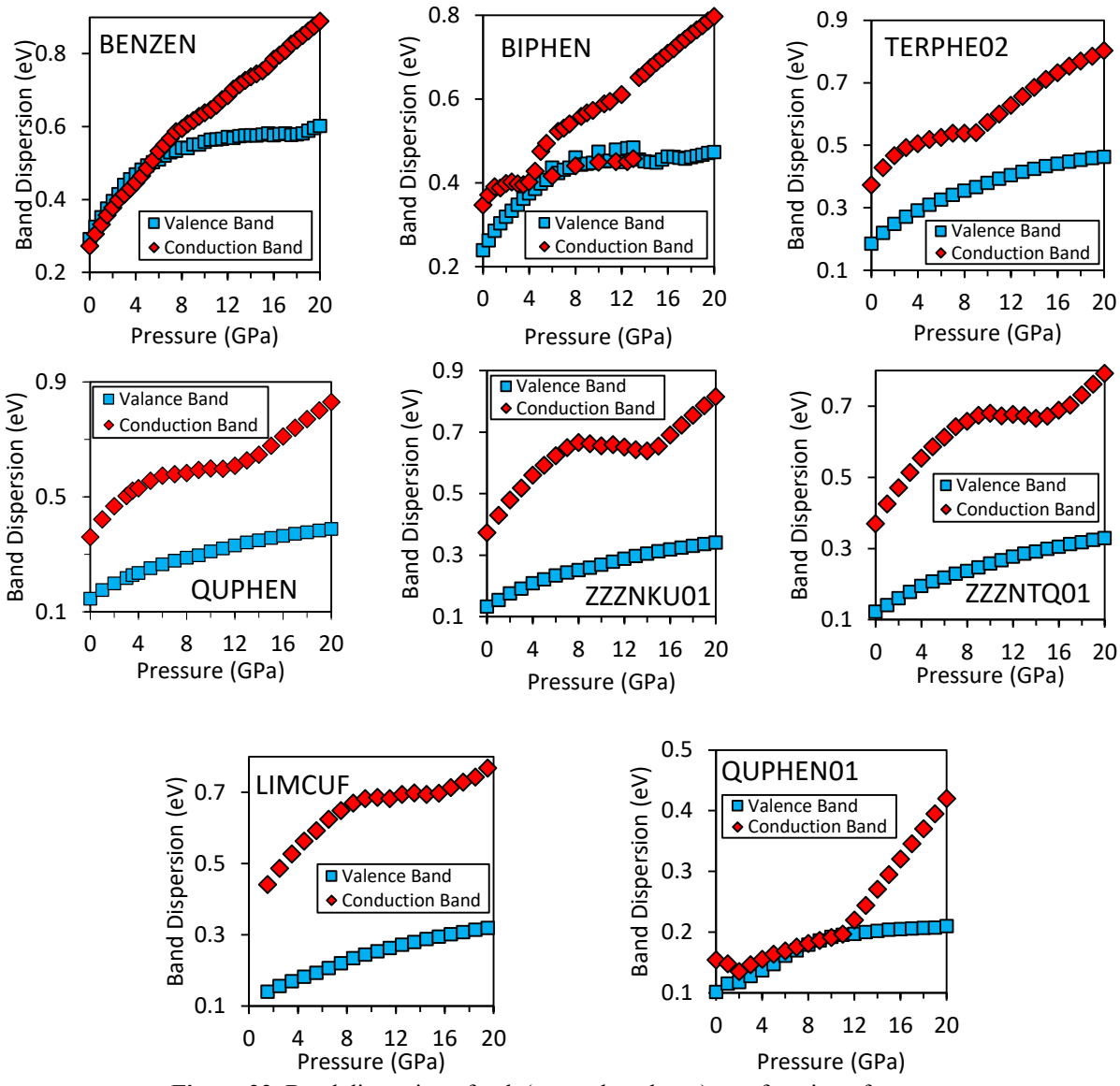


Figure 22. Band dispersion of poly(para-phenylenes) as a function of pressure

For *para*-quaterphenyl, the monoclinic (QUPHEN) and triclinic (QUPHEN01) polymorphs exhibit significantly different bandwidth pressure dependence. This may be attributed to differences in the pressure dependent changes associated with the intermolecular interactions of each polymorph, as visible in the decomposed percent area of the Hirshfeld surfaces in **Fig 23**. In the monoclinic polymorph the molecular conformation is planar and the crystal exhibits no C···C contacts on the Hirshfeld surface. Under pressure, the C···C contacts increase, whereas the C···H and H···H contacts decrease. This results in a structure that maintains *n*-type behavior across all pressures, accompanied by conduction and valence bandwidth increases across the entire pressure range. In contrast, in the triclinic phase, the molecules adopt a twisted conformation and the crystal structure has some C···C intermolecular contacts at 0 GPa. When pressure is applied, the molecules become planar by ~0.5 GPa, similar to *para*-terphenyl^{73,74}. This results in rearrangement of the crystal matrix as demonstrated by the *decrease* in the C···C contacts up to ~ 2 GPa in **Fig 23**. The flattening of the molecules and

decrease in C···C contacts correlates with the decrease in the conduction band dispersion in **Fig 22**. Above 3 GPa the C···C contacts increase nearly linearly up to 20 GPa. As a result of the aforementioned molecular and crystalline changes, the triclinic polymorph is initially an *n*-type semiconductor, then it becomes ambipolar, and finally reverts to *n*-type behavior at higher pressures.

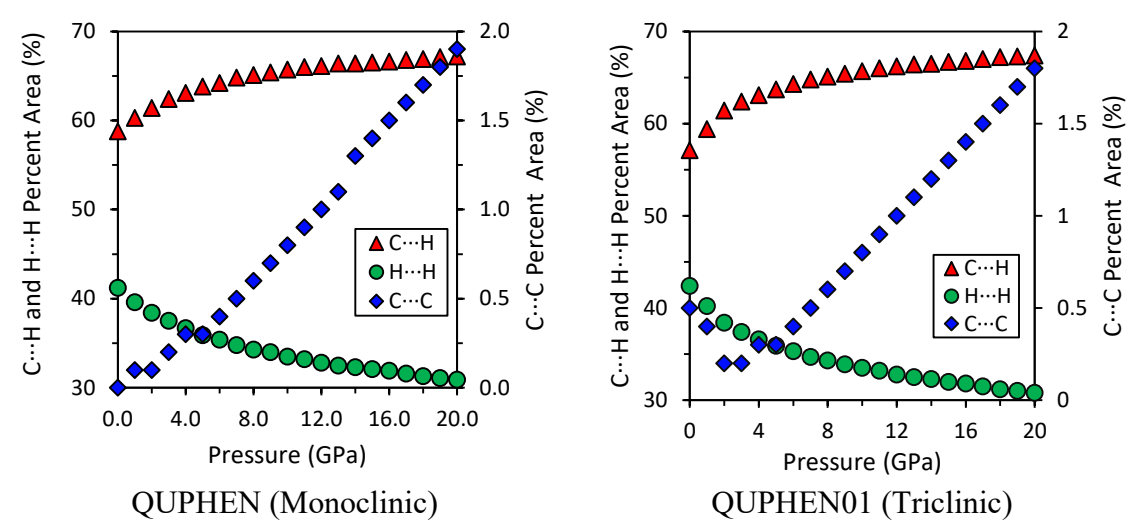


Figure 23. Percent close contact area on the Hirshfeld surface as a function of pressure for monoclinic (QUPHEN) and triclinic (QUPHEN01) *para*-quaterphenyl.

4.0. Conclusion

In the second part of this two-part study, we investigated the influence of isotropic pressure up to 20 GPa on the electronic properties of 42 polycyclic aromatic hydrocarbons that crystallize in a herringbone motif (HB-PAHs), using dispersion-inclusive density functional theory (DFT+vdW). It was found that in most cases the PBE derived band gap (E_g^{PBE}) decreases with pressure in a continuous manner. The continuous narrowing of E_g^{PBE} may be primarily attributed to increased coupling of the frontier molecular orbitals as the density of the materials increases. However, discontinuities in pressure dependent E_q^{PBE} behavior were observed for six structures (CENYAV, KAGFOP, FANNUL, ABECAL, SANQII, and DBPHEN02). The discontinuities may be attributed to changes not only in the intermolecular coupling, but also in the molecular conformation, resulting in changes to the bandwidths as well as band origin energies (i.e., the single molecule HOMO and LUMO energies). Most systems were found to maintain their direct/indirect nature and their n- or p-type polarity over the entire pressure range. However, in some cases the evolution of the band structure under pressure leads to direct/indirect transitions and polarity switching. We conclude that the band gap, polarity, and direct/indirect nature of the band gap of HB-PAHs may be manipulated by applying pressure and altering the intermolecular close contacts and the electronic coupling of the frontier molecular orbitals. The ability to tune these electronic properties is a promising route for optimizing the performance of organic semiconductors for applications in optoelectronic devices.

Acknowledgements

Work at CPP by BS was funded by National Science Foundation (NSF) Division of Materials Research through grant DMR-1637026. NM acknowledges support from the NSF Division of Materials Research through grant DMR-1554428.

Supporting Information Available: [...]

References

- (1) Wang, C.; Dong, H.; Hu, W.; Liu, Y.; Zhu, D. Semiconducting π-Conjugated Systems in Field-Effect Transistors: A Material Odyssey of Organic Electronics. *Chem. Rev.* 2012, 112 (4), 2208–2267.
- (2) Feng, X.; Marcon, V.; Pisula, W.; Hansen, M. R.; Kirkpatrick, J.; Grozema, F.; Andrienko, D.; Kremer, K.; Müllen, K. Towards High Charge-Carrier Mobilities by Rational Design of the Shape and Periphery of Discotics. *Nat. Mater.* **2009**, *8* (5), 421–426.
- (3) Mitsuhashi, R.; Suzuki, Y.; Yamanari, Y.; Mitamura, H.; Kambe, T.; Ikeda, N.; Okamoto, H.; Fujiwara, A.; Yamaji, M.; Kawasaki, N.; et al. Superconductivity in Alkali-Metal-Doped Picene. *Nature* **2010**, *464* (7285), 76–79.
- (4) Rieger, R.; Mullen, K. Forever Young: Polycyclic Aromatic Hydrocarbons as Model Cases for Structural and Optical Studies. *J. Phys. Org. Chem.* **2010**, *23* (4), 315–325.
- (5) Wang, X. F.; Liu, R. H.; Gui, Z.; Xie, Y. L.; Yan, Y. J.; Ying, J. J.; Luo, X. G.; Chen, X. H. Superconductivity at 5 K in Alkali-Metal-Doped Phenanthrene. *Nat. Commun.* **2011**, *2*, 507.
- (6) Xue, M.; Cao, T.; Wang, D.; Wu, Y.; Yang, H.; Dong, X.; He, J.; Li, F.; Chen, G. F. Superconductivity above 30 K in Alkali-Metal-Doped Hydrocarbon. *Sci. Rep.* **2012**, *2*, 389.
- (7) Thejo Kalyani, N.; Dhoble, S. J. Organic Light Emitting Diodes: Energy Saving Lighting Technology A Review. *Renew. Sustain. Energy Rev.* **2012**, *16* (5), 2696–2723.
- (8) Brütting, W.; Frischeisen, J.; Schmidt, T. D.; Scholz, B. J.; Mayr, C. Device Efficiency of Organic Light-Emitting Diodes: Progress by Improved Light Outcoupling. *Phys. Status Solidi Appl. Mater. Sci.* **2013**, *210* (1), 44–65.
- (9) Torsi, L.; Magliulo, M.; Manoli, K.; Palazzo, G. Organic Field-Effect Transistor Sensors: A Tutorial Review. *Chem. Soc. Rev.* **2013**, *42* (22), 8612–8628.
- (10) Sirringhaus, H. 25th Anniversary Article: Organic Field-Effect Transistors: The Path beyond Amorphous Silicon. *Adv. Mater.* **2014**, *26* (9), 1319–1335.
- (11) Hedley, G. J.; Ruseckas, A.; Samuel, I. D. W. Light Harvesting for Organic Photovoltaics. *Chem. Rev.* **2017**, *117* (2), 796–837.
- (12) Mazzio, K. A.; Luscombe, C. K. The Future of Organic Photovoltaics. *Chem. Soc. Rev.* **2015**, *44* (1), 78–90.
- (13) Sun, S.-S.; Dalton, L. R. *Introduction to Organic Electronic and Optoelectronic Materials and Devices*; CRC Press, 2008.
- (14) Ostroverkhova, O. Handbook of Organic Materials for Optical and (Opto)Electronic Devices: Properties and Applications; Woodhead Publishing Ltd, 2013.
- (15) Radisavljevic, I.; Marjanovic, D.; Novakovic, N.; Ivanovic, N. Changes in Structure and Properties of Oligophenylenes under Selected External Influences. *Mater. Sci. Forum* **2007**, *555*, 509–514.
- (16) Fanetti, S.; Citroni, M.; Malavasi, L.; Artioli, G. A.; Postorino, P.; Bini, R. High-Pressure Optical Properties and Chemical Stability of Picene. *J. Phys. Chem. C* **2013**, *117* (10), 5343–5351.
- (17) Schatschneider, B.; Monaco, S.; Tkatchenko, A.; Liang, J.-J. Understanding the Structure and Electronic Properties of Molecular Crystals Under Pressure: Application of Dispersion Corrected DFT to Oligoacenes. *J. Phys. Chem. A* **2013**, *117* (34), 8323–8331.

- (18) Xiao, L.-P.; Zhong, G.-H.; Zeng, Z.; Chen, X.-J. Theoretical Study on Structural and Electronic Properties of Solid Anthracene under High Pressure by Density Functional Theory. *Mol. Phys.* **2016**, *114* (2), 283–289.
- (19) Zhao, X.-M.; Zhong, G.-H.; Zhang, J.; Huang, Q.-W.; Goncharov, A. F.; Lin, H.-Q.; Chen, X.-J. Combined Experimental and Computational Study of High-Pressure Behavior of Triphenylene. *Sci. Rep.* **2016**, *6* (1), 25600.
- (20) Wang, X.; Garcia, T.; Monaco, S.; Schatschneider, B.; Marom, N. Effect of Crystal Packing on the Excitonic Properties of Rubrene Polymorphs. *CrystEngComm* **2016**, *18* (38), 7353–7362.
- (21) Casati, N.; Kleppe, A.; Jephcoat, A. P.; Macchi, P.; Boehler, R. Putting Pressure on Aromaticity along with in Situ Experimental Electron Density of a Molecular Crystal. *Nat. Commun.* **2016**, *7*, 10901.
- (22) Rang, Z.; Haraldsson, A.; Kim, D. M.; Ruden, P. P.; Nathan, M. I.; Chesterfield, R. J.; Frisbie, C. D. Hydrostatic-Pressure Dependence of the Photoconductivity of Single-Crystal Pentacene and Tetracene. *Appl. Phys. Lett.* **2001**, *79* (17), 2731–2733.
- (23) Liu, C.; Bard, A. J. Pressure-Induced Insulator–conductor Transition in a Photoconducting Organic Liquid-Crystal Film. *Nature* **2002**, *418* (6894), 162–164.
- (24) Fabbiani, F. P. A.; Allan, D. R.; Parsons, S.; Pulham, C. R. Exploration of the High-Pressure Behaviour of Polycyclic Aromatic Hydrocarbons: Naphthalene, Phenanthrene and Pyrene. *Acta Crystallogr. Sect. B Struct. Sci.* **2006**, *62* (5), 826–842.
- (25) Wang, L. J.; Li, Q. K.; Shuai, Z. Effects of Pressure and Temperature on the Carrier Transports in Organic Crystal: A First-Principles Study. *J. Chem. Phys.* **2008**, *128* (19), 194706.
- (26) Nguyen, T. P.; Shim, J. H. Hydrostatic Pressure Effect on Charge Transport Properties of Phenacene Organic Semiconductors. *Phys. Chem. Chem. Phys.* **2016**, *18* (20), 13888–13896.
- (27) Cai, W.; Zhang, R.; Yao, Y.; Deemyad, S.; Piezochromism and Structural and Electronic Properties of Benz[a]Anthracene under Pressure. *Phys. Chem. Chem. Phys.* **2017**, *19* (8), 6216–6223.
- (28) Schatschneider, B.; Phelps, J.; Jezowski, S. A New Parameter for Classification of Polycyclic Aromatic Hydrocarbon Crystalline Motifs: A Hirshfeld Surface Investigation. *CrystEngComm* **2011**, *13* (24), 7216.
- (29) Desiraju, G. R.; Gavezzotti, A. From Molecular to Crystal Structure; Polynuclear Aromatic Hydrocarbons. *J. Chem. Soc. Chem. Commun.* **1989**, No. 10, 621.
- (30) Desiraju, G. R.; Gavezzotti, A. Crystal Structures of Polynuclear Aromatic Hydrocarbons. Classification, Rationalization and Prediction from Molecular Structure. *Acta Crystallogr. Sect. B Struct. Sci.* **1989**, *45* (5), 473–482.
- (31) Desiraju, G. R. Crystal Engineering: The Design of Organic Solids; Elsevier, 1989.
- (32) Schatschneider, B.; Liang, J. J. Simulated Pressure Response of Crystalline Indole. *J. Chem. Phys.* **2011**, *135* (16), 164508.
- (33) Huang, Q.-W.; Zhang, J.; Berlie, A.; Qin, Z.-X.; Zhao, X.-M.; Zhang, J.-B.; Tang, L.-Y.; Liu, J.; Zhang, C.; Zhong, G.-H.; Lin, H. Q.; Chen, X. J. Structural and Vibrational Properties of Phenanthrene under Pressure. *J. Chem. Phys.* **2013**, *139* (139).
- (34) Liu, T.; Xu, S.; Sun, C.; Zhou, M. Raman Spectroscopic Studies on P-Terphenyl under High Pressure. *Chem. Phys. Lett.* **2014**, *615*, 1–5.
- (35) Capitani, F.; Höppner, M.; Malavasi, L.; Marini, C.; Artioli, G. A.; Hanfland, M.; Dore,

- P.; Boeri, L.; Postorino, P. Structural Evolution of Solid Phenanthrene at High Pressures. J. Phys. Chem. C 2016, 120 (26), 14310–14316.
- (36) Hammouri, M.; Garcia, T. M.; Cook, C.; Marom, N.; Schatschneider, B. High-Throughput Pressure Dependent DFT Investigation of Herringbone Polycyclic Aromatic Hydrocarbons (HB-PAHs): Part 1. Pressure Dependent Structure Trends. *J. Phys. Chem. C* 2018 (in review).
- (37) Perdew, J. P.; Burke, K.; Ernzerhof, M. Generalized Gradient Approximation Made Simple. *Phys. Rev. Lett.* **1996**, *77* (18), 3865–3868.
- (38) Tkatchenko, A.; Scheffler, M. Accurate Molecular Van Der Waals Interactions from Ground-State Electron Density and Free-Atom Reference Data. *Phys. Rev. Lett.* **2009**, *102* (7), 073005.
- (39) Schatschneider, B.; Monaco, S.; Liang, J.-J.; Tkatchenko, A. High-Throughput Investigation of the Geometry and Electronic Structures of Gas-Phase and Crystalline Polycyclic Aromatic Hydrocarbons. *J. Phys. Chem. C* **2014**, *118* (34), 19964–19974.
- (40) Schatschneider, B.; Liang, J.-J.; Jezowski, S.; Tkatchenko, A. Phase Transition between Cubic and Monoclinic Polymorphs of the Tetracyanoethylene Crystal: The Role of Temperature and Kinetics. *CrystEngComm* **2012**, *14* (14), 4656.
- (41) Adamo, C.; Barone, V. Toward Reliable Density Functional Methods without Adjustable Parameters: The PBE0 Model. *J. Chem. Phys.* **1999**.
- (42) Clark, S. J.; Segall II, M. D.; Pickard II, C. J.; Hasnip III, P. J.; J Probert IV, M. I.; Refson, K. V; Payne, M. C. First Principles Methods Using CASTEP. *Z. fur Krystallographie* **2005**, *220*, 567-570.
- (43) Monkhorst, H. J.; Pack, J. D. Special Points for Brillouin-Zone Integrations. *Phys. Rev. B* **1976**, *13* (12), 5188–5192.
- (44) Rappe, A. M.; Rabe, K. M.; Kaxiras, E.; Joannopoulos, J. D. Optimized Pseudopotentials. *Phys. Rev. B* **1990**, *41* (2), 1227–1230.
- (45) Pfrommer, B. G.; Côté, M.; Louie, S. G.; Cohen, M. L. Relaxation of Crystals with the Quasi-Newton Method. *J. Comput. Phys.* **1997**, *131* (1), 233–240.
- (46) S.K. Wolff, D.J. Grimwood, J.J. McKinnon, M.J. Turner, D. Jayatilaka, M.A. Spackman, University of Western Australia, 2012. CrystalExplorer (Version 3.1). *Chemical Communications*. 2007, p 3814.
- (47) Wood, P. A.; McKinnon, J. J.; Parsons, S.; Pidcock, E.; Spackman, M. A. Analysis of the Compression of Molecular Crystal Structures Using Hirshfeld Surfaces. *CrystEngComm* **2008**, *10* (4), 368–376.
- (48) Spackman, M. a.; Jayatilaka, D. Hirshfeld Surface Analysis. CrystEngComm 2009, 11, 19.
- (49) McKinnon, J. J.; Jayatilaka, D.; Spackman, M. A. Towards Quantitative Analysis of Intermolecular Interactions with Hirshfeld Surfaces. *Chem. Commun.* **2007**, No. 37, 3814–3816.
- (50) Yan, D.; Evans, D. G. Molecular Crystalline Materials with Tunable Luminescent Properties: From Polymorphs to Multi-Component Solids. *Mater. Horiz.* **2014**, *1* (1), 46–57.
- (51) Coropceanu, V.; Cornil, J.; da Silva Filho, D. A.; Olivier, Y.; Silbey, R.; Brédas, J. L. Charge Transport in Organic Semiconductors. *Chem. Rev.* **2007**, *107* (4), 926–952.
- (52) Brédas, J.-L.; Beljonne, D.; Coropceanu, V.; Cornil, J. Charge-Transfer and Energy-Transfer Processes in π-Conjugated Oligomers and Polymers: A Molecular Picture. *Chem. Rev.* **2004**, *104*, 4971–5003.

- (53) Hoffmann, R. Solids and Surfaces. A Chemist's View of Bonding in Extended Structures., 1st ed.; VCH Publishers Inc., 1990; Vol. 168.
- (54) Li, Y.; Coropceanu, V.; Brédas, J. L. Thermal Narrowing of the Electronic Bandwidths in Organic Molecular Semiconductors: Impact of the Crystal Thermal Expansion. *J. Phys. Chem. Lett.* **2012**, *3* (22), 3325–3329.
- (55) Marsh, R. E.; Clemente, D. A. A Survey of Crystal Structures Published in the Journal of the American Chemical Society. *Inorganica Chim. Acta* **2007**, *360* (14), 4017–4024.
- (56) Chiang, C. C.; Paul, I. C. Crystal and Molecular Structure of [14] Annulene. *J. Am. Chem. Soc.* **1972**, *94* (13), 4741–4743.
- (57) Kao, K.-C. Dielectric Phenomena in Solids: With Emphasis on Physical Concepts of Electronic Processes; Academic Press, 2004.
- (58) Joshi, N. V. Photoconductivity: Art, Science, and Technology; Marcel Dekker, 1990.
- (59) Neville, R. C. Solar Energy Conversion: The Solar Cell; Elsevier, 1995.
- (60) Mazer, J. A. Solar Cells: An Introduction to Crystalline Photovoltaic Technology; Kluwer Academic Publishers, 1997.
- (61) Oberhofer, H.; Reuter, K.; Blumberger, J. Charge Transport in Molecular Materials: An Assessment of Computational Methods. *Chem. Rev.* **2017**, *117* (15), 10319–10357.
- (62) Schober, C.; Reuter, K.; Oberhofer, H. Virtual Screening for High Carrier Mobility in Organic Semiconductors. *J. Phys. Chem. Lett.* **2016**, *7* (19), 3973–3977.
- (63) Brédas, J. L.; Calbert, J. P.; da Silva Filho, D. A.; Cornil, J. Organic Semiconductors: A Theoretical Characterization of the Basic Parameters Governing Charge Transport. *Proc. Natl. Acad. Sci. U. S. A.* **2002**, *99* (9), 5804–5809.
- (64) Duke, C. B.; Schein, L. B. Organic Solids: Is Energy-band Theory Enough? *Phys. Today* **1980**, *33* (2), 42–48.
- (65) Wu, M. W.; Conwell, E. M. Transport in α-Sexithiophene Films. *Chem. Phys. Lett.* **1997**, *266* (3–4), 363–367.
- (66) Jurchescu, O. D.; Baas, J.; Palstra, T. T. M. Effect of Impurities on the Mobility of Single Crystal Pentacene. *Appl. Phys. Lett.* **2004**, *84* (16), 3061–3063.
- (67) Warta, W.; Stehle, R.; Karl, N. Ultrapure, High Mobility Organic Photoconductors. *Appl. Phys. A Solids Surfaces* **1985**, *36* (3), 163–170.
- (68) Fichou, D.; Structural Order in Conjugated Oligothiophenes and Its Implications on Opto-Electronic Devices. *J. Mater. Chem.* **2000**, *10* (3), 571–588.
- (69) Rang, Z.; Nathan, M. I.; Ruden, P. P.; Chesterfield, R.; Frisbie, C. D. Hydrostatic-Pressure Dependence of Organic Thin-Film Transistor Current versus Voltage Characteristics. *Appl. Phys. Lett.* **2004**, *85* (23), 5760–5762.
- (70) Rang, Z.; Nathan, M. I.; Paul, P. Hydrostatic Pressure Dependence of Charge Carrier Transport in Single-Crystal Rubrene Devices. *Appl. Phys. Lett.* **2005**, *86* (101).
- (71) Hummer, K.; Ambrosch-Draxl, C. Electronic Properties of Oligoacenes from First Principles. *Phys. Rev. B* **2005**, *72* (20), 205205.
- (72) Rang, Z.; Nathan, M. I.; Ruden, P. P. Hydrostatic Pressure Dependence of Charge Carrier Transport in Single-Crystal Rubrene Devices. *Appl. Phys. Lett.* **2005**, *86* (12), 1–3.
- (73) Schatschneider, B.; Chronister, E. L. High-Resolution FTIR Study of the Para-Terphenyl Phase Transition at High Pressure. *J. Lumin.* **2007**, *127* (1), 34–40.
- (74) Schatschneider, B.; Chronister, E. L. Molecular Dynamics Simulations of Temperature-and Pressure-Induced Solid-Solid Phase Transitions in Crystalline Para-Terphenyl. *Mol. Simul.* **2008**, *34* (10–15), 1159–1166.